SCIENCE CHINA PRESS

SCIENCE CHINA Life Sciences
life.scichina.com link.springer.com
https://doi.org/10.1007/s11427-023-2557-x

RESEARCH PAPER

Dynamic intrauterine crosstalk promotes porcine embryo implantation during early pregnancy

Xupeng Zang[1,2], Shengchen Gu[1,2], Wenjing Wang[1,2], Junsong Shi[3], Jianyu Gan[1,2], Qun Hu[1,2], Chen Zhou[1,2], Yue Ding[1,2], Yanjuan He[1,2], Lei Jiang[1], Ting Gu[1,2,5], Zheng Xu[1,2,5], Sixiu Huang[1,2,5], Huaqiang Yang[1,2,5], Fanming Meng[4], Zicong Li[1,2,5], Gengyuan Cai[1,2,5], Linjun Hong[1,2,5*] & Zhenfang Wu[1,2,3,5*]

[1]State Key Laboratory of Swine and Poultry Breeding Industry, National Engineering Research Center for Breeding Swine Industry, College of Animal Science, South China Agricultural University, Guangzhou 510642, China;
[2]Guangdong Provincial Key Laboratory of Agro-Animal Genomics and Molecular Breeding, South China Agricultural University, Guangzhou 510642, China;
[3]Yunfu Subcenter of Guangdong Laboratory for Lingnan Modern Agriculture, Yunfu 527300, China;
[4]Guangdong Key Laboratory of Animal Breeding and Nutrition, Institute of Animal Science, Guangdong Academy of Agricultural Sciences, Guangzhou 510640, China
[5]Key Laboratory of South China Modern Biological Seed Industry, Ministry of Agriculture and Rural Affairs, Guangzhou 510520, China

*Corresponding authors (Linjun Hong, email: linjun.hong@scau.edu.cn; Zhenfang Wu, email: wzfemail@163.com)

Received 18 January 2024; Accepted 21 February 2024; Published online 11 May 2024

Dynamic crosstalk between the embryo and mother is crucial during implantation. Here, we comprehensively profile the single-cell transcriptome of pig peri-implantation embryos and corresponding maternal endometrium, identifying 4 different lineages in embryos and 13 cell types in the endometrium. Cell-specific gene expression characterizes 4 distinct trophectoderm subpopulations, showing development from undifferentiated trophectoderm to polar and mural trophectoderm. Dynamic expression of genes in different types of endometrial cells illustrates their molecular response to embryos during implantation. Then, we developed a novel tool, ExtraCellTalk, generating an overall dynamic map of maternal-foetal crosstalk using uterine luminal proteins as bridges. Through cross-species comparisons, we identified a conserved RBP4/STRA6 pathway in which embryonic-derived RBP4 could target the STRA6 receptor on stromal cells to regulate the interaction with other endometrial cells. These results provide insight into the maternal-foetal crosstalk during embryo implantation and represent a valuable resource for further studies to improve embryo implantation.

endometrial remodeling | ExtraCellTalk | implantation | maternal-foetal crosstalk | trophoblast

INTRODUCTION

Embryo implantation is critical to a successful pregnancy, and approximately 75% of pregnancy losses result from implantation failure (Wilcox et al., 1988). Successful implantation depends on well-orchestrated crosstalk between the embryo and maternal uterus, whereby the timely development of an embryo is synchronized with the receptive endometrium (Dey et al., 2004). Studies have shown that defects in maternal-foetal crosstalk contribute to a wide range of pregnancy disorders, including preeclampsia, recurrent pregnancy failure, and even infertility (Arck and Hecher, 2013; Zhu et al., 2024). With the advancement of modern medicine, *in vitro* fertilization and embryo transfer have made significant progress towards overcoming infertility, but the implantation rate is low due to the inability to establish proper crosstalk between the embryo and mother, greatly limiting the extensive application of this technology (Carson and Kallen, 2021; Corachán et al., 2021). Therefore, a comprehensive understanding of maternal-foetal crosstalk is of great importance for investigating the mysteries of embryo implantation to address this global reproductive problem.

Due to experimental difficulties and ethical restrictions, the current understanding of human maternal-foetal crosstalk is rooted mainly in *in-vitro* models of human cells and animal studies, particularly in mice. Several recent studies have revealed cellular crosstalk at the early maternal-foetal interface by collecting human decidua tissue and utilizing developed single-cell sequencing techniques (Suryawanshi et al., 2018; Vento-Tormo et al., 2018). However, these studies still have not fully elucidated the dynamic crosstalk between embryo and the mother during embryo implantation. For the specific purpose of this study, *in vitro* cell experiments are not suitable for studying the embryo-maternal crosstalk during implantation. Furthermore, a single animal model, such as only mice, can limit our understanding of unique perspectives on the real regulatory mechanisms of embryo implantation due to differences between species, thus requiring additional animals for the study. In addition to mice, another excellent animal model for human medicine is pigs, because pigs are similar to humans in terms of anatomy, physiology, organ size, and cell cycle characteristics (Jin et al., 2022; Lunney et al., 2021; Zhu et al., 2022), and pig embryos are thought to be closer to humans than rodents in pre-gastrulation development (Ramos-Ibeas et al., 2019), which is usually the initial stage of embryo implantation.

After fertilization occurs, the pig embryo moves from the oviduct into uterine lumen on approximately day 2 of pregnancy and develops into a blastocyst by day 5 of pregnancy. The blastocyst hatches from the zona pellucida on days 6 to 7 of pregnancy and further expands. Subsequently, the pig embryo develops into the peri-implantation stage of embryo implanta-

tion, and its morphology undergoes significant changes, elongating rapidly from the 2 to 6 mm spherical embryo on day 9 of pregnancy to the 150 to 200 mm long filamentous embryo on day 12 of pregnancy. Eventually, the elongated embryo contacts the maternal endometrium on days 15–16 of pregnancy, ending the free state of the embryo in the uterine lumen (Bazer and Johnson, 2014; Mattson et al., 1990). On day 12 of pregnancy, a large amount of estrogen is synthesized and released by the pig embryo, and the maternal endometrium response is stimulated by estrogen. Accompanied by various cytokines and signals between embryos and the mother, abundant maternal-foetal crosstalk induces a gradual transition of the endometrium from non-receptive to receptive, which is considered a critical stage for maternal recognition of pregnancy (Bazer et al., 2009b; Geisert et al., 2017).

Therefore, in this study, we performed single-cell sequencing analysis of embryos and corresponding endometrial tissue on day 9 of pregnancy (the initial stage of embryo implantation) and day 12 of pregnancy (the stage of maternal pregnancy recognition with abundant maternal-foetal crosstalk). We developed a novel tool, ExtraCellTalk, that comprehensively analyzes the crosstalk between embryos and the maternal uterus during implantation, mediated by uterine luminal proteins of the same stages. Subsequently, through cross-species comparisons of pigs, mice, and humans, we identified some features conserved across species during maternal-foetal crosstalk. These analyses shed new insights into maternal-foetal crosstalk during implantation and refine the understanding of the molecular mechanisms of embryo implantation, thereby providing critical resources for future studies to develop effective strategies to improve the ability of clinicians to treat infertility, to prevent pregnancy loss and to develop novel contraceptive approaches.

RESULTS

Single-cell sequencing delineates lineage segregation in peri-implantation pig embryos

To elucidate the crosstalk between embryos and the maternal uterus during implantation, we first collected peri-implantation pig embryos on days 9 and 12 of pregnancy and performed single-cell transcriptome sequencing (Figure 1A and B). We identified epiblast (EPI), primitive endoderm (PrE) and trophectoderm (TE) cells in pig peri-implantation embryos using marker genes, including *OCT4* and *IGFBP2* for EPI, *GATA4* and *GATA6* for PrE, and *GATA2* and *GATA3* for TE (Figure S1A in Supporting Information). Subsequently, we further determined the EPI, PrE and TE lineages in pig embryos using previously defined embryonic germ layer gene signatures (Zhi et al., 2022) (Figure 1C). The three lineages occupied distinct regions in the unsupervised clustered UMAP space, with no clustering bias in embryos on days 9 and 12 of pregnancy (Figure 1D; Figure S1B in Supporting Information). In addition to these three embryonic lineages, we found another lineage that occupies a large position in UMAP (Figure 1D). Notably, this lineage did not express lineage-specific markers of early embryos (Figure 1E). Cell-state trajectory analysis suggested that the lineage could potentially transition into three other embryonic lineages (Figure 1F). While evaluating the three lineage scores for all embryonic cells, we found that the lineage was in an intermediate transitional state among the three embryonic lineages, which we named the intermediate (IM) lineage (Figure 1D; Figure S1B and C in Supporting Information). Indeed, the IM lineage is ubiquitous in induced blastocysts in both humans and mice, which suggests that it may be a transitional state germ layer lineage specification (Li et al., 2019; Liu et al., 2021b; Wu et al., 2024; Yu et al., 2021). Using protein immunofluorescence, we validated lineage-specific marker genes in peri-implantation embryos and visualized the spatial distribution of these cells *in situ*. We found the expression of lineage-specific markers in embryo corresponding positions, but some cells did not express these markers, confirming the presence of the IM lineage we identified (Figure 1H–M).

Based on gene differential expression analysis, we highlighted the most significantly enriched genes for each lineage (Figure S1E in Supporting Information). We performed GO enrichment and KEGG pathway analysis on the top 50 differentially expressed genes identified in each lineage, and the results showed consistent lineage-specific biological function (Figure S2 in Supporting Information), with PrE enriched for endoderm development, TE for negative regulation of actin filament polymerization and estrogen signalling pathway, and EPI for signalling pathways regulating pluripotency of stem cells. Interestingly, we found that those differential genes identified by the intermediate transition state lineage IM were involved in only some metabolic processes, including protein, lipid, and energy metabolism. Nevertheless, they had a higher transcriptional complexity than other lineages (Figure S1F and G in Supporting Information), suggesting that lineage transitions may require precise and complex regulation and abundant physiological metabolic activities to provide them with the necessary energy and substances. With the progress of development, EPI can gradually differentiate into ectoderm and mesoderm, and the embryo transitions from three germ layers into a state of 4 germ layers (Rossant and Tam, 2022). We found that pig EPIs on days 9 and 12 of pregnancy expressed some mesoderm markers, such as *HAND1*, *VIM* and *BMP4*, and subsequent analysis indicated that EPIs at these stages may have initiated differentiation into mesoderm and ectoderm (Figure S3 in Supporting Information).

We compared the pseudo-bulk data generated from single-cell transcriptomes with our published bulk transcriptome data of the same stages (Zang et al., 2021) and found high concordance (Figure 1G). Next, we compared our data with previously published single-cell transcriptomic data from pig embryos (Liu et al., 2021a; Zhi et al., 2022). For the same pregnancy stages, our data clustered well with those of Zhi et al. but varied dramatically from those of Liu et al. (Figure S4A in Supporting Information), which may be due to different sampling methods. Liu et al. isolated embryonic lineages by mechanical manipulation, whereas we and Zhi et al. both obtained single cells by tissue enzymolysis. Furthermore, since EPI is relatively conserved across mammalian species and an important source of embryonic stem cells (Brons et al., 2007), we also compared data from mouse and human embryos at different developmental stages (Mohammed et al., 2017; Zhou et al., 2019). We found that pig EPI on days 9 and 12 of pregnancy was highly correlated with mouse embryonic day 4.5 (E4.5) and E5.5 EPI (Figure S4B in Supporting Information). Similar to previous studies (Liu et al., 2021a), pig EPI was more similar to human E8–E12 EPIs (Figure S4C in Supporting Information). To minimize bias from stage mismatches across species, we first compared EPI development between pigs and E4.5 and E5.5 mice based on the results of

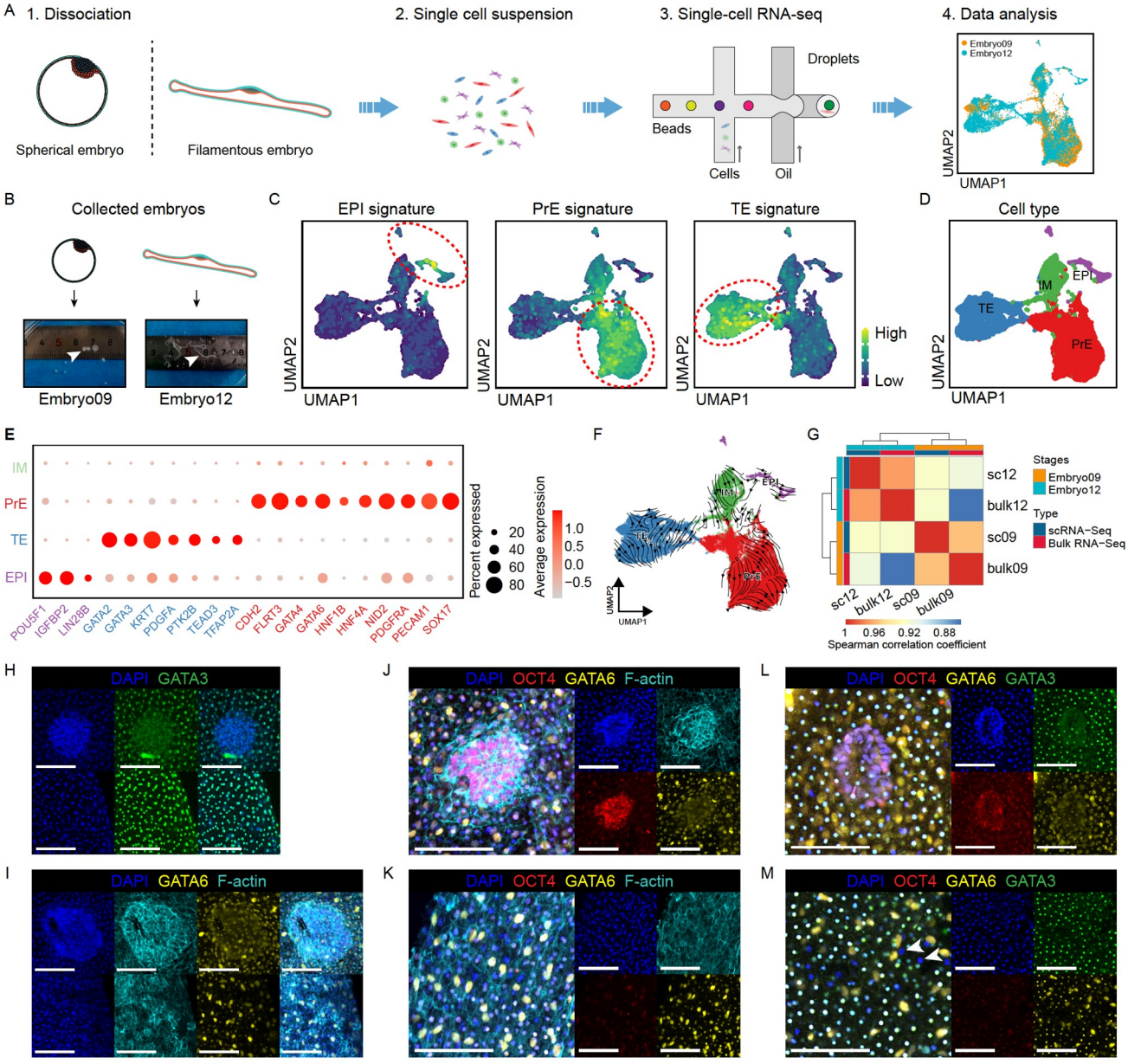

Figure 1. Single-cell transcriptomic profiling of pig peri-implantation embryos. A, Experimental workflow for pig embryos scRNA-seq. B, Representative images of pig embryos used in this study. Arrows showing spherical embryo on day 9 and filamentous embryo on day 12 of pregnancy, respectively. C, Per-cell expression score for EPI, PrE, and TE signatures on UMAP of pig embryos scRNA-seq dataset. D, Cells derived from peri-implantation embryos are coloured by lineage score: EPI (purple), PrE (red), TE (blue) and IM (green). E, Dot plots indicating the expression of well-known markers in each embryo lineage. F, Pseudo-time analysis of RNA velocity in pig embryo cells, arrows predicting directions of the cell trajectories. G, Correlation analysis of merged embryo cells compared with our previously published bulk embryo transcriptomes (Zang et al., 2021). H–M, Representative immunofluorescence costaining images of POU5F1/OCT4 (EPI), GATA6 (PrE), GATA3 (TE) and F-actin in pig embryos on day 9 of pregnancy. All scale bars, 100 μm.

correlation analyses. Heatmap of differentially expressed genes revealed obvious highly expressed genes in pigs and mice (Figure S4D in Supporting Information). GO enrichment and KEGG pathway analyses showed that highly expressed genes in mice were enriched in biological processes such as cell cycle and protein metabolism. In contrast, genes highly expressed in pigs were enriched in cell migration and immune response (Figure S4E and F in Supporting Information). Next, we compared EPI development in pigs and humans (E8–E12). Interestingly, some genes that were highly expressed in pigs compared with mice were also found in humans (Figure S4G in Supporting Information). GO enrichment and KEGG pathway analyses also revealed that highly expressed genes in humans were involved in cell cycle and metabolism processes, while those in pigs related to some RNA processes and hormone synthesis (Figure S4H and I in Supporting Information). Overall, EPI in pig embryo peri-implantation stage more closely resembles the three germ-layer developmental stages of mouse and human embryonic development, which precedes gastrulation (Niakan et al., 2012). This again demonstrates the conservation of embryonic development during implantation even though the implantation pattern differs widely between species, with human and mouse embryos

implanting in uterine wall and pig embryos apposed to the maternal endometrium (Turco and Moffett, 2019).

Development of the trophoblast lineage

Because embryo-maternal crosstalk exists mainly between the TE and maternal uterus during implantation, our downstream analysis was focused mainly on the TE lineage. The trophoblasts of pig embryos on day 12 of pregnancy could synthesize a large amount of oestrogen, which is considered an important signal for maternal-foetal pregnancy recognition (Bazer and Johnson, 2014). By analyzing the key genes of estrogen synthesis in these TE cells, we found their expression levels were visibly different, suggesting that these TE cells may have distinct subpopulations (Figure S5A in Supporting Information). Therefore, we reclustered the obtained TE lineage, visualized all cells using tSNE, and identified four distinct subpopulations (Figure 2A). Previous studies reported that TE cells can specifically develop into polar and mural TE during embryogenesis (Petropoulos et al., 2016). By examining the expression of polar and mural TE canonical markers in TE cells and calculating a signature score for each TE cell (Liu et al., 2021b), we found that only three TE subpopulations expressed these markers (Figure 2B; Figure S5B in Supporting Information). Notably, these 3 subpopulations were abundantly present on day 12 of pregnancy (Figure 2C and D), while another subpopulation that was in embryos mainly on day 9 had dramatically different characteristics (Figure 2E; Figure S1D in Supporting Information). Subsequently, we identified differentially expressed genes in distinct TE subpopulations (Figure S5C and D in Supporting Information) and performed GO enrichment and KEGG pathway analysis. We found that in addition to one mural TE subpopulation enriched in some inflammatory processes, such as positive regulation of interleukin-1 production and the IL-17 signalling pathway, the other three TE subpopulations are involved in numerous metabolic-related regulatory processes (Figure 2F; Figure S5E in Supporting Information). Based on the features obtained, we named the identified four TE subpopulations undifferentiated TE (udTE), polar TE (pTE), inflammatory mural TE (imTE), and metabolic mural TE (mmTE) (Figure 2A). In addition to oestrogen, pig embryos on day 12 of pregnancy synthesize a large amount of IFNG (Figure S5F and G in Supporting Information), which is believed to regulate maternal immune responses to establish pregnancy (McLendon et al., 2020). Unlike humans or rodents, pig peri-implantation embryos undergo a dramatic elongation of the TE (Bazer and Johnson, 2014), causing the embryo to transition from a spherical embryo on day 9 of pregnancy to a filamentous embryo on day 12 of pregnancy (Figure 1B). The elongation does not involve cellular hyperplasia, but is caused by alterations in microfilaments and junctional complexes of TE (Bazer and Johnson, 2014; Mattson et al., 1990). Among these four populations of TE cells, only imTE subpopulation was enriched for the regulation of the actin cytoskeleton (Figure 2F), suggesting that the TE subpopulation may regulate the morphological transformation of embryos at this stage. Considering the transcriptomic differences between polar TE and mural TE, we analyzed the molecular characteristics of two large TE subpopulations in pigs (Figure 2G and H). These differentially expressed genes were significantly enriched in some metabolic processes and the regulation of supramolecular fiber organization in actin cytoskeleton, further revealing that pTE and mTE play different roles in embryonic development and morphological transformation during implantation.

Dynamic gene expression of different TE subpopulations was traced from days 9 to 12 of pregnancy (Figure S6 in Supporting Information). The results showed that there were obviously changes in gene expression during embryo implantation among different TE subpopulations, but a considerable number of genes were still shared during the process. For example, one of the critical pro-inflammatory cytokines, IL1B2, was highly expressed on day 9 of pregnancy in all four TE subpopulations and is necessary for morphological transition in pig embryos (Whyte et al., 2018). To confirm the developmental trajectories of these TE subpopulations, we performed cell-state trajectory analysis and pseudotime analysis. Consistent with our hypothesis, the udTE subpopulation from embryos on day 9 of pregnancy could transdevelop into pTE and mTE (including imTE and mmTE) (Figure 2I and J; Figure S5H in Supporting Information). Additionally, we identified some genes potentially regulating the transdevelopment of the udTE subpopulation, including the unrecognized functional genes *ENSSCG00000029160* and *HES1*, which may regulate udTE to pTE, and *SGPP1* and *HSP90B1*, which may regulate udTE to mTE (Figure S5I and J in Supporting Information). We compared the stem cell scores of the different TE subpopulations. Interestingly, we found that the stem cell scores of the transitioned pTE and mTE subpopulations were higher than those of the pre-transitioned udTE subpopulation (Figure 2K and L), which seems to contradict the state of stem cell differentiation, and the more primitive udTE should have a higher stem cell score. Transdevelopment of TE cells is also orchestrated by a sophisticated network of transcription factors (TFs); therefore, we evaluated the activities of the TF regulatory network in each TE subpopulation using pySCENIC (Figure 2M and N). We found that PBX1 and JUNB were highly active and specifically expressed in the regulatory network of the pTE subpopulation, suggesting that they may be the important TFs regulating this transdevelopmental pathway (Figure 2O and P). The TFs identified by the other three TE subpopulations also had high activity levels and expression levels within their subpopulations, showing potential regulation of corresponding transdevelopmental pathways (Figure S5K–M in Supporting Information). Furthermore, previous studies have shown that epigenetic modifications are essential in early embryonic development (Smith and Meissner, 2013). We found that the expression of *DNMT1*, a key gene for maintaining DNA methylation (Lyko, 2018), did not change significantly in the four TE subpopulations, whereas the expression level of *DNMT3B*, a key gene for *de novo* DNA methylation synthesis, was significantly increased in the three transitioned TE populations, indicating that the transdevelopment of TE cells requires the coparticipation of epigenetic modifications including DNA methylation modifications (Figure 2Q and R).

Cellular heterogeneity in the peri-implantation endometrium

To characterize the dynamic intrauterine crosstalk between embryos and the maternal uterus during implantation, we need to focus on the endometrium at this stage in addition to the developing embryo. Therefore, we collected corresponding endometrial tissues and performed single-cell transcriptome sequencing (Figure 3A). After unbiased clustering and dimen-

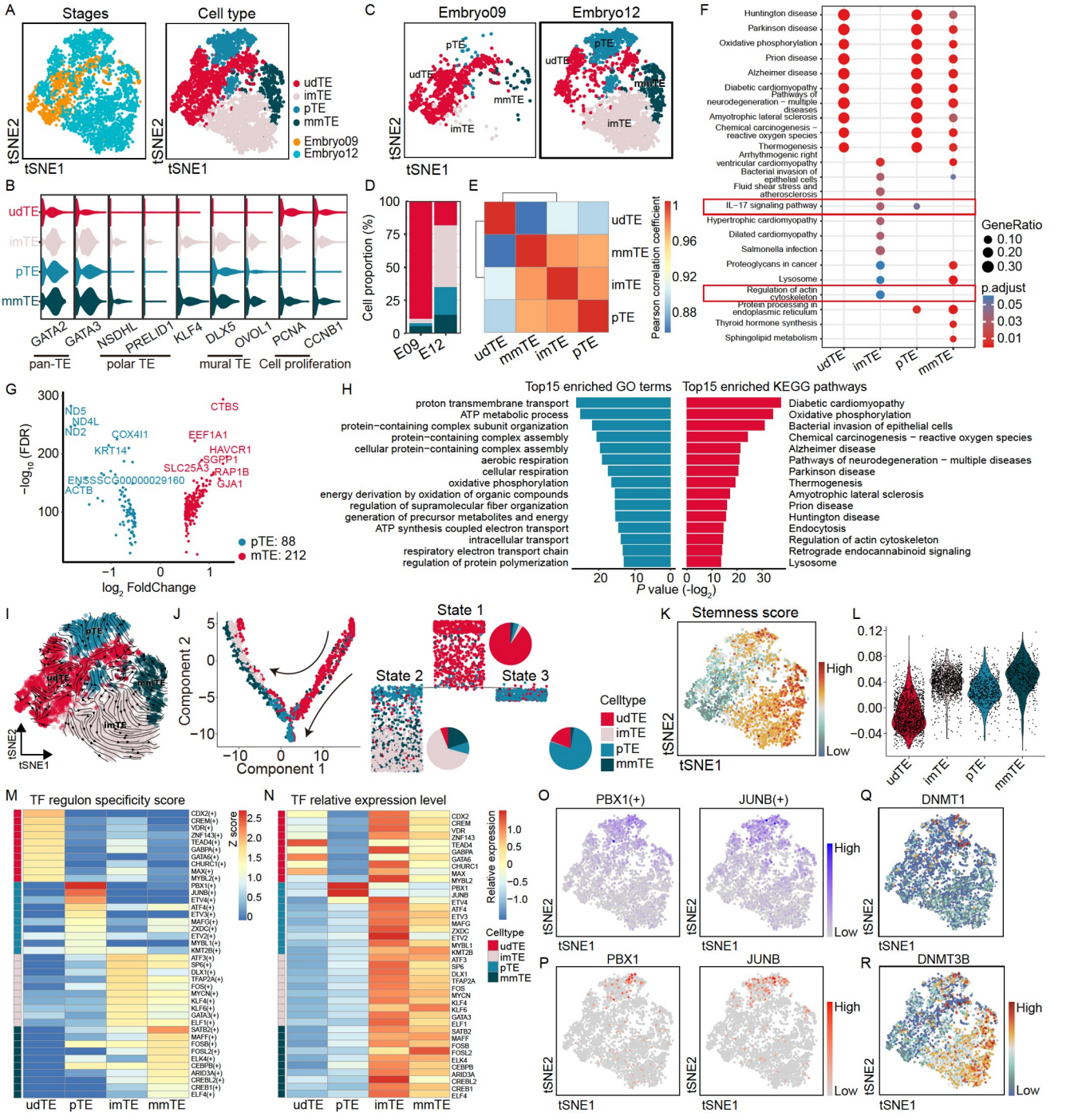

Figure 2. Dynamic development of the embryonic trophoblast during implantation. A, tSNE visualization of TE subpopulations. TE cells are subdivided into udTE, pTE, imTE and mmTE. B, Violin plots showing the expression level of marker genes in distinct TE subpopulations. C, The distribution of TE subpopulations in embryos on days 9 and 12 of pregnancy. D, The proportion of each TE subpopulation in embryos on days 9 and 12 of pregnancy. E, Correlation analysis of different TE subpopulations. F, KEGG pathway analysis of differentially expressed genes in TE subpopulations. G, Volcano plots showing differentially expressed genes between pTE and mTE. H, GO enrichment and KEGG pathway analysis of differentially expressed genes between pTE and mTE, showing the top 15 enriched terms for each category. I, Pseudo-time analysis of RNA velocity in TE cells, arrows predicting directions of the pseudo-time. J, Monocle2 prediction of TE developmental trajectory with pseudo-time, with cells colored by different cell subpopulations to which they belong. K, Per TE cell expression score for stemness signature on tSNE. L, Stemness scores for each TE subpopulation by violin plots. M, Heatmap displaying normalized activity of top 10 TF regulons in each TE subpopulation predicted by pySCENIC. N, Heatmap displaying relative expression levels of the top 10 TF genes. O and P, UMAP plots highlighting the activity (M) and expression levels (N) of PBX1 and JUNB in pTE. Q and R, UMAPs showing expression levels of DNA methyl modification key genes *DNMT1* (O) and *DNMT3B* (P) in TE cells.

sionality reduction, these endometrial cells were divided into 13 different endometrial cell populations using some typical marker genes, including 6 populations of immune cells and 7 populations of nonimmune cells (Figure 3B; Figure S7A and B in Supporting

https://doi.org/10.1007/s11427-023-2557-x

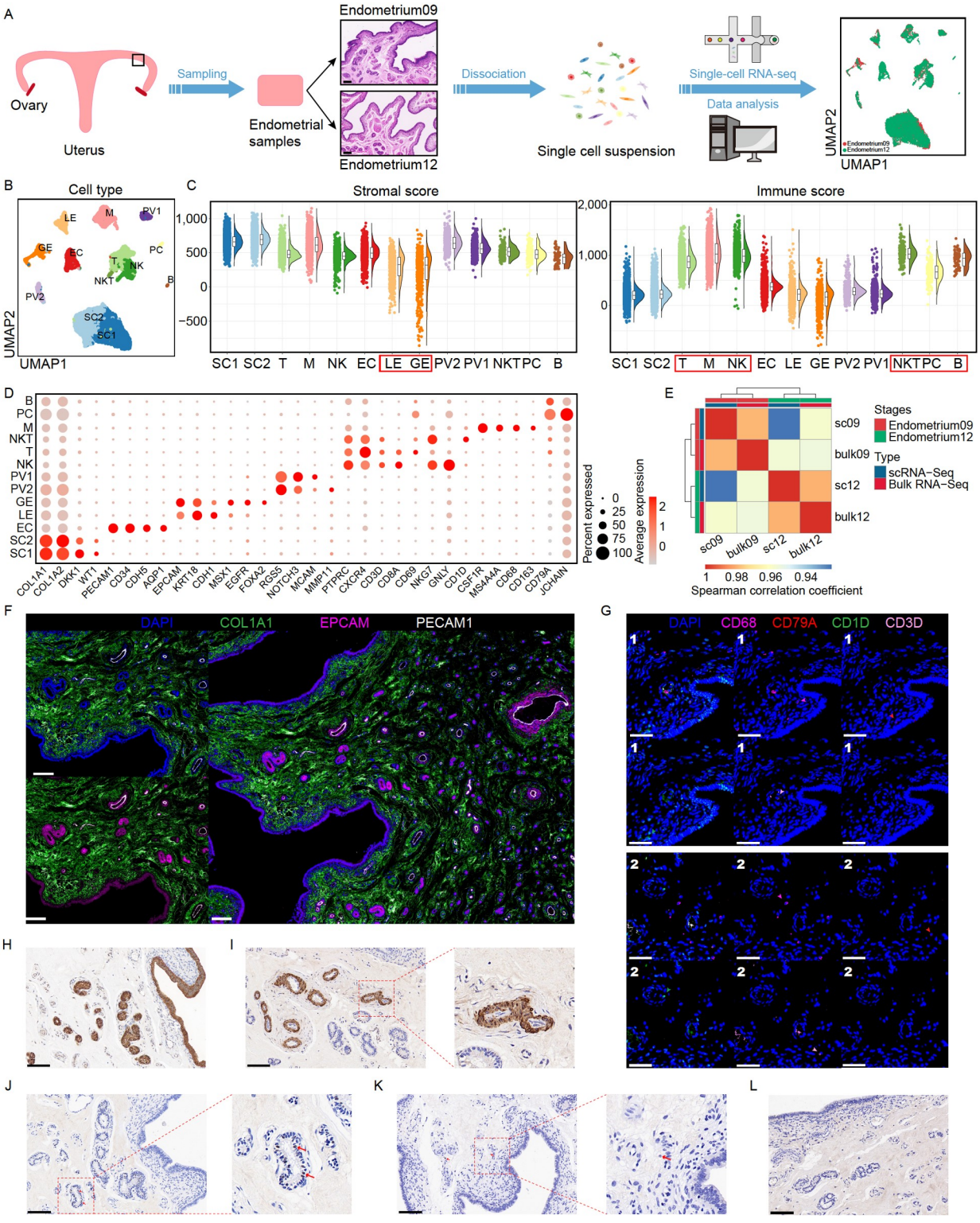

Figure 3. Characterization of different cell types in pig peri-implantation endometrium. A, Schematic representation of the pig endometrium scRNA-seq analysis. B, UMAP of cells coloured by associated cell types in pig endometrium. B, B cells; EC, endothelial cells; M, macrophages; NK, natural killer cells; NKT, natural killer T cells; PC, plasma cells; PV, perivascular cells; SC, stromal cells; T, T cells. C, Stromal and immune scoring of endometrial non-immune and immune cells. D, Dot plots showing the expressed and coexpressed classical marker genes of each cell type. E, Correlation analysis of merged endometrium cells compared with published bulk transcriptomes (Wang et al., 2016) from peri-implantation endometrium. F, Representative immunofluorescence costaining images of nonimmune cells in pig endometrium on day 9 of pregnancy. COL1A1, stromal cells; EPCAM, epithelial cells; PECAM1, endothelial cells. Scale bar, 100 μm. G, Representative immunofluorescence costaining images of immune cells in pig endometrium on day 9 of pregnancy. CD68, macrophages; CD79A, B cells; CD1D, NKT cells; CD3D, NK and T cells. Scale bar, 100 μm. H–L, Immunohistochemistry of differential genes in diverse endometrial cells on day 9 of pregnancy, stained for ANXA4 (H, LE and GE cells), ACTA2 (I, PV1 and PV2 cells), FOXJ1 (J, ciliated epithelial cells), GATA3 (K, NKT, NK and T cells), and VEGFD (L, SC1 and SC2 cells). Scale bar, 100 μm.

Information). To validate the identified endometrial cell populations, we calculated stromal and immune cell scores for different cell types and found that the scores were consistent with the corresponding cell population types (Figure 3C). Moreover, the canonical markers were specifically expressed in the different types of endometrial cells we identified, demonstrating the accuracy of endometrial cell types (Figure 3D). Then, we performed gene differential expression analysis on these distinct endometrial cells and identified some novel cell type-specific marker genes (Figure S7C in Supporting Information). Based on the GO enrichment and KEGG pathway analysis of the top 50 differentially expressed genes for each cell type, we found that different types of cells play diverse biological functions in the peri-implantation endometrium (Figure S8 in Supporting Information). Notably, endometrial type 1 stromal cells were enriched for several biological processes related to reproductive system development. Similar to the embryos, the pseudobulk data of endometrial cells were highly concordant with previously published bulk endometrium data on days 9 and 12 of pregnancy (Wang et al., 2016) (Figure 3E). By analysing the similarities of different cell populations in two stages of the endometrium, we found that except for NK, M and B cells, the differences in other cells were relatively small (Figure S7D in Supporting Information), implying that these immune cells may may be involved in maternal-foetal pregnancy recognition.

To locate the distinct endometrial cell populations *in situ*, we used immunofluorescence for selected canonical markers on serial sections of the uterus. These experiments confirm that EPCAM+ epithelial cells and PECAM1+ endothelial cells are located between COL1A1+ stromal cells, while various immune cells are scattered in the endometrium (Figure 3Fand G; Figure S9A and B in Supporting Information). In addition, we visualized the localization of some identified novel markers on uterine sections using immunohistochemistry (Figure S9C and D in Supporting Information). Consistent with the results displayed by canonical markers, these novel markers were also expressed on corresponding cells (Figure 3H–L; Figure S9E–I in Supporting Information). Interestingly, a typical marker of ciliated epithelium, FOXJ1, was not expressed in the luminal epithelium (LE) of pigs as it was in humans and rodents but was expressed in glandular epithelium (GE), where it may play a different role (Figure 3J; Figure S9G in Supporting Information).

Endometrial response to embryo during implantation

Next, we traced the dynamic expression pattern of different endometrial cell types between days 9 and 12 of pregnancy. LE and GE exhibited the most differentially expressed genes (Figure 4A), consistent with their importance during embryo implantation (Bazer et al., 2009a). Among them, genes differentially expressed in LE were significantly enriched in biological processes such as placental development and cell migration regulation (Figure 4B and C), indicating that it is remodeling to form a receptive endometrium for embryo implantation (Sun et al., 2022). Interestingly, we found that these genes were enriched in the labyrinthine layer development (Figure 4C), which is a vital event in the development of mouse placenta (Ochiai et al., 2022), showing that even if there are large differences between species, underlying conservation is still in endometrium and placenta development during implantation. Two types of cell subpopulations were obtained by reclustering LE, with marker genes differentially expressed (Figure 4D and E). LE1 mainly carried out some activities related to energy metabolism, while LE2 was involved in cell migration and localization (Figure 4F), which may be an important functional cell subpopulation during implantation. The genes dynamically expressed in GE between days 9 and 12 of pregnancy were enriched in the biosynthesis and metabolic processes of peptides (Figure 4G and H), which is consistent with the large number of substances secreted by GE at this stage to establish uterine receptivity and embryo implantation (Gray et al., 2001). Likewise, GE could be divided into two cell subpopulations (Figure 4I and J). It is worth noting that GE1 performed the secretory function of GE, and the GE2 subpopulation is the ciliated GE identified above (Figure 4K). In the analysis of the identified important endometrial type 1 stromal cells, we found that differential genes in SC1 between days 9 and 12 of pregnancy were enriched in the biological process of innate immune response (Figure S9J and K in Supporting Information). Some chemokines, such as CXCL10, which was upregulated on day 12 of pregnancy, could recruit immune cells (Du et al., 2014). NK cells respond to the recruitment and jointly establish a maternal immune-tolerant microenvironment to promote embryo implantation and pregnancy (Figure S9L and M in Supporting Information) (Albini and Noonan, 2021; Du et al., 2014).

Bidirectional functional mechanisms of uterine luminal free proteins and extracellular vesicle encapsulated proteins

Previous studies have shown that multiple cytokines and extracellular vesicles in the microenvironment of the maternal-foetal interface mediate precise crosstalk between the embryo and mother during pregnancy (Du et al., 2014; Machtinger et al., 2016). During the implantation process of pig embryos, since these embryos are free in the uterine lumen, the crosstalk between embryos and the mother could be mediated by the contents in the uterine lumen (Bazer and Johnson, 2014; Kaczmarek et al., 2020). Our recent study found that there are abundant proteins in the uterine lumen during implantation of pig embryo implantation and these proteins exist in two different forms, one free in the uterine lumen and the other encapsulated by extracellular vesicles (He et al., 2022; Hong et al., 2023). Therefore, we comprehensively compared data on these two different forms of proteins to evaluate their bidirectional functional mechanisms in maternal-foetal crosstalk.

In this study, we analyzed free and extracellular vesicle-encapsulated proteins identified by iTRAQ proteomics technology from pig uterine lumen on days 9 and 12 of pregnancy. Based on the comparison of total identified proteins, we found that not all proteins were specifically free from the uterine lumen or encapsulated by extracellular vesicles, and a considerable number of proteins coexisted in both forms (Figure 5A). We first analysed changes in the abundance of proteins coexisting with free proteins and the extracellular-vesicle-encapsulated proteins in the uterine lumen in two stages (Figure 5B; Figure S10A in Supporting Information). Since day 9 is at the beginning of the pig embryo implantation, and day 12 is a critical stage for maternal pregnancy recognition (Bazer et al., 2009b; Geisert et al., 2017). Thus, compared with those on day 9 of pregnancy, proteins whose abundance was upregulated on day 12 of pregnancy may be involved in regulating embryo implantation.

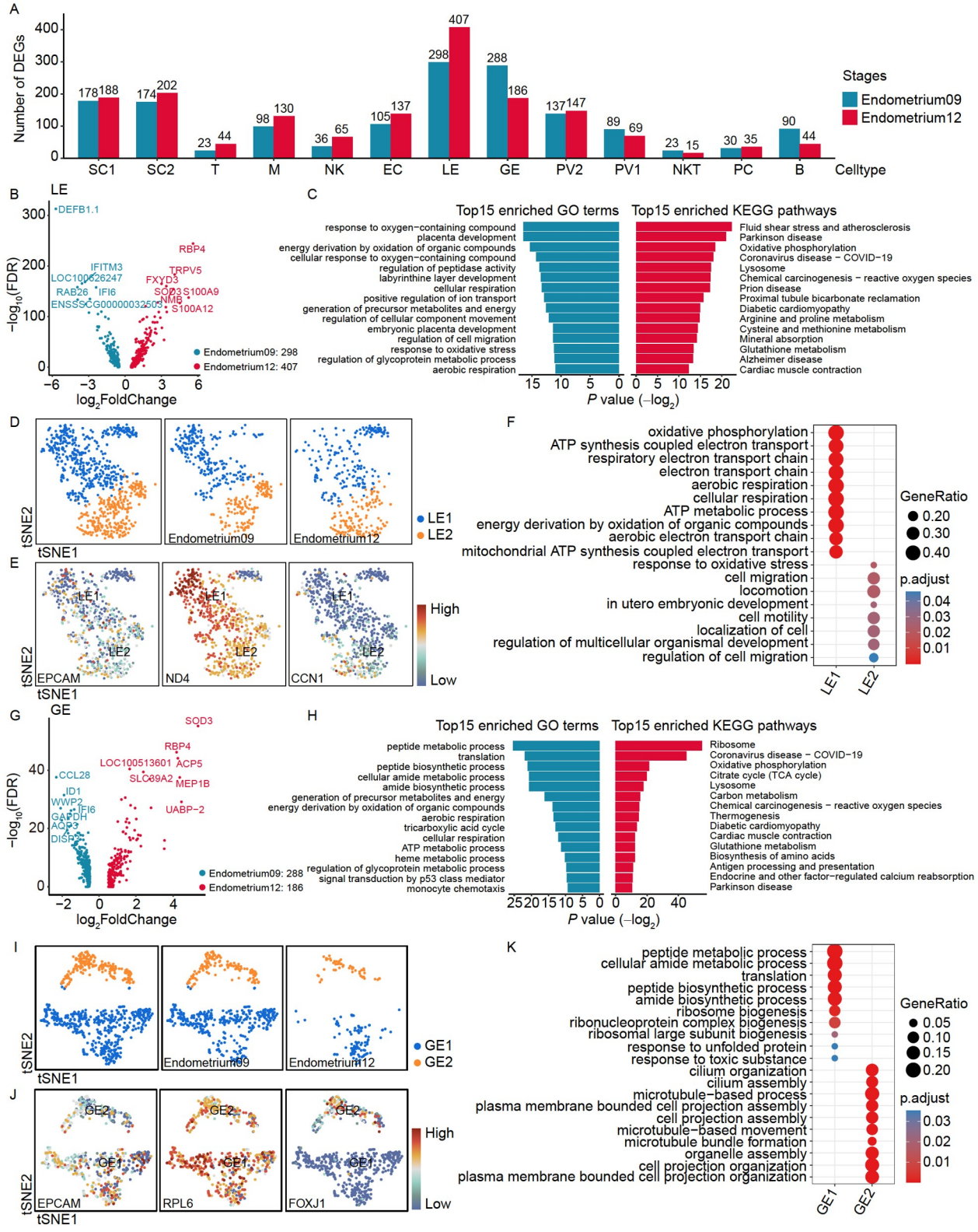

Figure 4. Dynamic gene expression of pig endometrial cells during implantation. A, Bar chart counting the number of differentially expressed genes for each endometrial cell type between days 9 and 12 of pregnancy. B, Volcano plots showing differentially expressed genes in LE between days 9 and 12 of pregnancy. C, GO enrichment and KEGG pathway analysis of differentially expressed genes in LE, showing the top 15 enriched terms for each category. D, tSNE visualization of LE subpopulations and distribution of LE subpopulations in the endometrium on days 9 and 12 of pregnancy. E, The distribution of *EPCAM*, *ND4*, and *CCN1* expression in LE cells on tSNE. F, GO enrichment analysis of differentially expressed genes in LE subpopulations. G, Volcano plots showing differentially expressed genes in GE between days 9 and 12 of pregnancy. H, GO enrichment and KEGG pathway analysis of differentially expressed genes in GE. I, tSNE visualization of GE subpopulations and distribution of GE subpopulations in the endometrium on days 9 and 12 of pregnancy. J, The distribution of *EPCAM*, *RPL6*, and *FOXJ1* expression in LE cells on tSNE. K, GO enrichment analysis of differentially expressed genes in GE subpopulations.

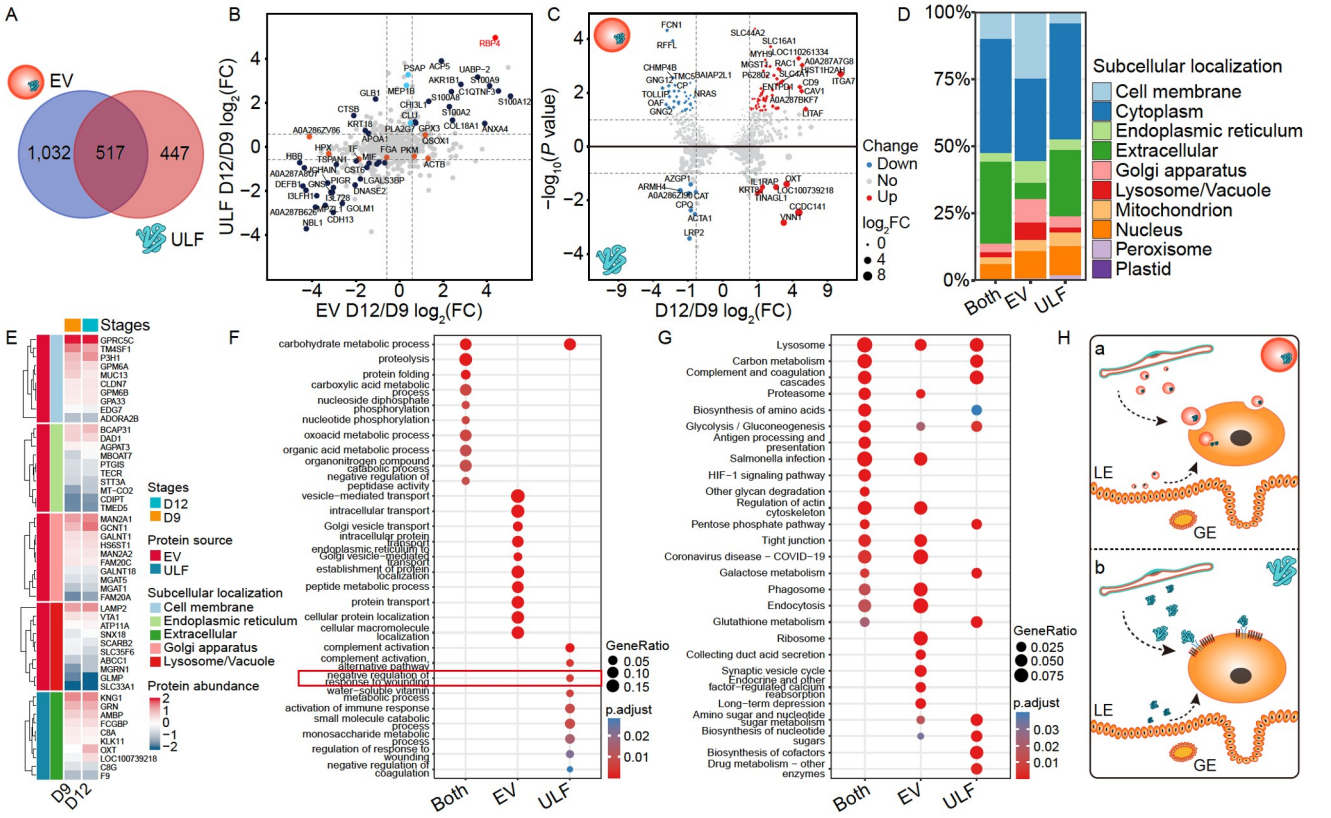

Figure 5. Comparison analysis of uterine luminal fluid free proteins and extracellular vesicle encapsulated proteins. A, Venn diagram comparing free proteins in uterine luminal fluid (ULF) and proteins encapsulated in extracellular vesicle (EV). B, Changes in ULF- and EV-source shared proteins on days 9 and 12 of pregnancy. C, Changes in ULF- and EV-source unique proteins on days 9 and 12 of pregnancy. D, Cellular sublocalization analysis of proteins among three classes proteins, including proteins shared by ULF and EV, proteins unique to EV, and proteins unique to ULF. E, Heatmap showing abundance changes between top 10 fractions of proteins with ULF and EV-specific cellular sublocalization between days 9 and 12 of pregnancy. F, GO enrichment analysis among three classes of proteins. G, KEGG pathway analysis among three classes proteins. H, Hypothesized diverse functional mechanisms of the two source proteins. (a) The proteins encapsulated in EVs directly fuses with cell membrane into cells and target cytoplasmic receptors to perform biological functions. (b) ULF free proteins perform their biological functions by binding to cell surface receptors. D9, day 9 of pregnancy; D12, day 12 of pregnancy.

For example, the inflammatory proteins S100A8 and S100A9 can regulate the expansion of myeloid-derived suppressor cells, which are vital to maintaining immunotolerance to the semi-allogeneic foetus for a successful pregnancy (He et al., 2018; Shi et al., 2021). Correspondingly, proteins that are free in the uterine lumen or encapsulated by extracellular vesicles perform their respective characteristic functions (Figure 5C; Figure S10B in Supporting Information). Due to the special vesicle structure of extracellular vesicles, most of their proteins are located in various biological membranes, while most of the free proteins are secreted proteins (Figure 5D and E). Subsequently, we performed GO enrichment and KEGG pathway analysis of the grouped proteins (Figure 5F and G). Unsurprisingly, the extracellular vesicle-specific proteins were enriched in several biological processes, such as vesicle-mediated cellular transport, consistent with their own functional mechanisms. Unique free proteins in the uterine lumen are involved in functional processes such as immune responses that contribute to maternal immune tolerance. Notably, we found enrichment in the wounding response process whose outcome seems to coincide with the endometrial remodelling required for this stage.

Overall, considering the functional mechanism of secreted proteins and extracellular vesicles (Colombo et al., 2014; Weis and Kobilka, 2018), we hypothesize (i) that extracellular vesicles in the uterine lumen could be secreted by embryos or endometrium, and transport the proteins encapsulated in them into the endometrium or embryos respectively, followed by targeting of the intracellular receptor to perform biological functions, and (ii) that free proteins in the uterine lumen could be secreted by embryos or endometrium to perform their biological functions by directly binding to receptors on the surfaces of endometrial cells or embryonic trophoblasts (Figure 5H).

Intrauterine crosstalk predicted by ExtraCellTalk

To systematically test the above hypotheses and characterize the dynamic crosstalk between embryos and the maternal uterus during implantation, we developed the ExtraCellTalk tool (Figure 6A). We first integrated ligand-receptor interacting pairs in some public databases, such as OmniPath (Türei et al., 2021), ICELLNET (Noël et al., 2021), CellChat (Jin et al., 2021), CEllCellInteractions (Ximerakis et al., 2019), and CellPhoneDB (Efremova et al., 2020). The comprehensive database of a priori ligand-receptor complexes formed the basis for subsequent computational approaches. We categorized proteins in the uterine lumen as ligands, considered receptor expression in different cell types among embryonic trophoblasts or in the endometrium, and used empirical shuffling to assess the cell-type-specific significance of ligand-receptor pairs (see Methods). Through cell membrane surface receptor-associated protein

https://doi.org/10.1007/s11427-023-2557-x

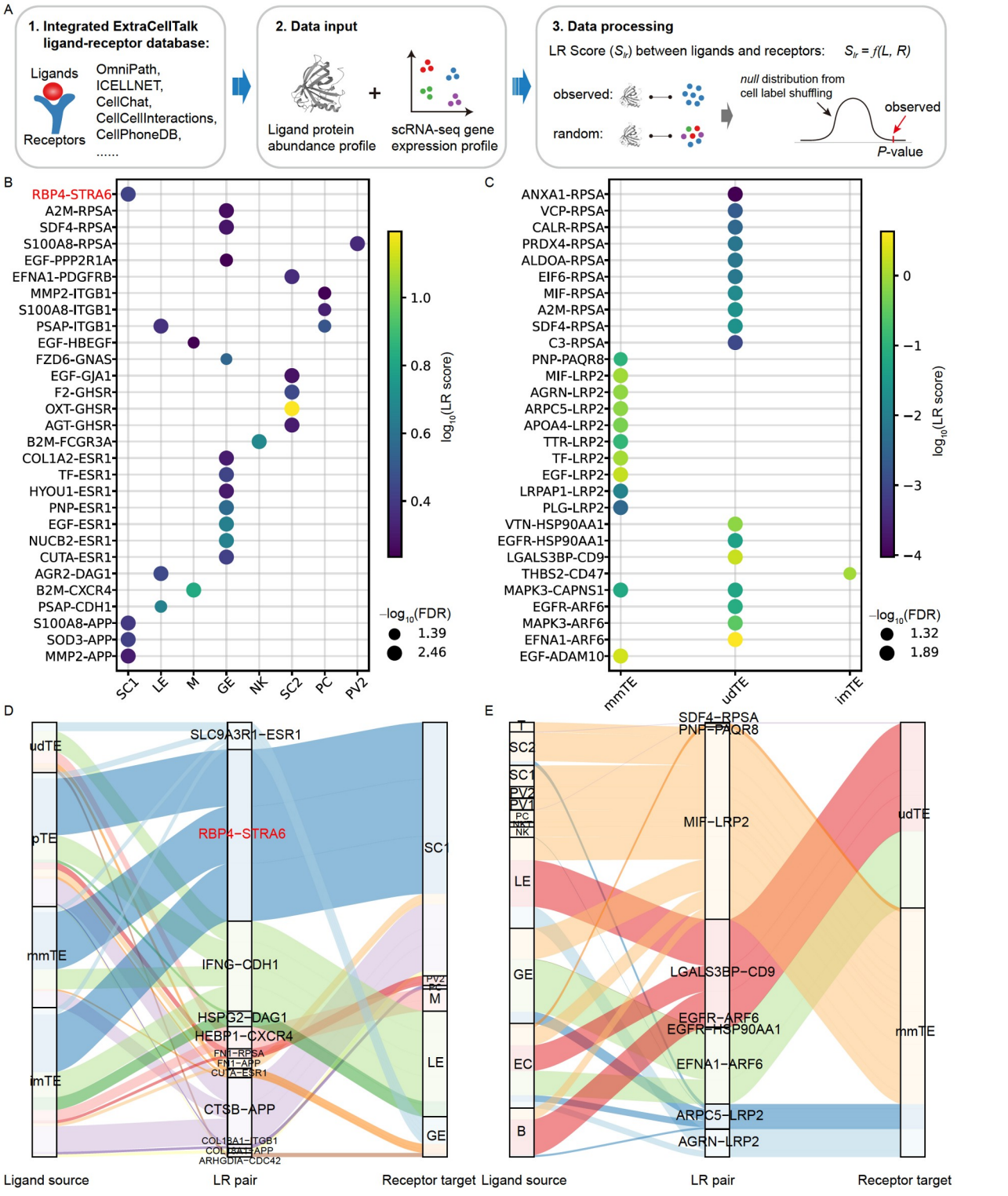

Figure 6. Extracellular-cell communication networks in intrauterine crosstalk between embryos and maternal uterus during implantation using ExtraCellTalk. A, Statistical framework for inferring specific extracellular ligand and celltype-receptor complexes from extracellular ligand protein abundance profile and single-cell transcriptomic data. The prior knowledge of ligand-receptor interacting pairs integrated from public ligand-receptor interacting pair databases was incorporated into ExtraCellTalk. Communication score (S_{lr}) is calculated using the product of fold changes in ligand and receptor. Recipient cells are randomly relabeled to generate a statistical *null* distribution to predict *P* values for a ligand–receptor complex using permutation tests (see Methods). B, Overview of the top 30 ligand-receptor interactions between uterine luminal free proteins and the endometrium. Corrected FDR values are indicated by the circle size, and S_{lr} between uterine cavity free protein and endometrial specific cell receptor are indicated by color. Analysis of receptors is performed at the mRNA level but extrapolated to the protein abundance level. C, Overview of the top 30 ligand-receptor interactions between uterine luminal free proteins and the embryo. D, Inferred communication patterns of embryo trophoblast-derived ligand signalling targeting specific endometrial cells via the uterine luminal free proteins. The thickness of the flow indicates the contribution of specific cell populations to each potential ligand-receptor interacting pair. E, Inferred communication patterns of endometrial-derived ligand signalling targeting specific embryo trophoblast cells via the uterine luminal free proteins.

complexes, we predicted the molecular interactions between uterine luminal fluid free proteins and trophoblast and endometrial cell surface receptors (Figure 6B and C; Table S1 in Supporting Information). Then, we expanded the corresponding source predictions of uterine luminal fluid-free proteins, that is, the ligand proteins acting on trophoblasts are hypothetically derived from endometrial cells, while the ligand proteins that want to function in the endometrium are considerately derived from trophoblast cells, yielding a potential cellular communication network between peri-implantation embryos and the maternal endometrium (Figure 6D and E; Table S2 in Supporting Information). For extracellular vesicle-encapsulated proteins, molecular interactions with intracellular receptors were predicted (Figure S11A, B and Table S3 in Supporting Information). We also expanded the source of these extracellular vesicles, generating a cellular communication network between peri-implantation embryos and the mother that was mediated by extracellular vesicles (Figure S11C, D and Table S4 in Supporting Information).

RBP4/STRA6 pathway promotes the interaction between endometrial stromal cells and other cells in intrauterine maternal-foetal crosstalk

Of the aforementioned predicted communication networks, the network with the highest communication score caught our attention: RBP4 signalling from polar and mural trophoblasts acts through uterine lumen binding to STRA6 on the surface of endometrial type 1 stromal cells (Figure 6B and D). To validate the identified RBP4/STRA6 pathway, we first confirmed the expression of RBP4 in the trophoblast lineage and found that it was almost all expressed in pTE or mTE subpopulations and nearly absent in the udTE subpopulation (Figure 7A and B). This resulted in little expression of RBP4 in trophoblasts on day 9 of pregnancy but abundant expression on day 12 of pregnancy (Figure 7C), which is consistent with the abovementioned abundance changes of RBP4 in the uterine lumen (Figure 5B). STRA6 is specifically expressed in endometrial stromal cells, and its expression increases significantly with pregnancy development only in type 1 stromal cells (Figure 7D–F), consistent with the coexpression relationship of the ligand-receptor complex. Previous studies have demonstrated the ligand-receptor binding relationship between RBP4 and STRA6 (Chen et al., 2016). We again used the latest AI tool AlphaFold2 to predict the binding domain between RBP4 and STRA6 (Figure 7G). The interaction relationship between RBP4 and STRA6 was revealed.

To explore the roles of the RBP4/STRA6 pathway during implantation, we intend to inject anti-Stra6 antibody into the uterus of mice to observe the result of blocking this pathway by inhibiting the activity of Stra6 receptor. However, due to species specificity, it is necessary to confirm whether the Rbp4/Stra6 pathway is conserved in mice. First, the amino acid sequence homology of RBP4 and STRA6 proteins was compared in pigs and mice, and their homology was relatively high (Figure 7H and I). We used previously published data on mouse embryos (Mohammed et al., 2017) and endometrium (Yang et al., 2021) during implantation to investigate the expression of Rbp4 in embryos and Stra6 in endometrium. To our delight, the expression level of Rbp4 in mouse embryos during implantation gradually increased with the progression of pregnancy, and Stra6 was also specifically expressed in mouse endometrial stromal cells, with the expression level being higher in the receptive endometrium (Figure S12A–G in Supporting Information). This suggests that we could use mice as a model to study the roles of the Rbp4/Stra6 pathway in intrauterine maternal-foetal crosstalk. Therefore, we injected anti-Stra6 into the preimplantation mouse uterus and found that after implantation at E6.5, the number of implanted embryos in mice was significantly reduced compared with that in controls (Figure 7J–L), which indicated that the Stra6 receptor regulates the embryo implantation process. Blocking Stra6 receptor activity in endometrial stromal cells disrupts maternal-foetal crosstalk, leading to pregnancy failure.

To characterize the underlying molecular mechanism of the Rbp4/Stra6 pathway, we collected decidua from these mice and first performed bulk transcriptome sequencing (Figure 7M). In contrast to that in the DPBS-injected control group, decidual changes were evident in anti-Stra6-injected mice (Figure 7N). In our analysis of the bulk transcriptome of decidua tissue, we identified a large number of significantly upregulated differentially expressed genes (Figure 7O and P), such as *Itih5*, which maintains extracellular matrix stabilization (Veeck et al., 2008), and *Mmp7*, which participates in the breakdown of extracellular matrix (Rohani and Parks, 2015), suggesting corresponding functional changes in stromal cells of decidua tissue following inhibition of Stra6 receptor activity. Subsequently, we performed GO enrichment and KEGG pathway analysis on these identified differentially expressed genes (Figure 7Q). The results indicated that the differentially expressed genes in decidua tissue might induce the re-remodelling of decidua by participating in biological processes related to stromal cells and blood vessels through the interaction between the extracellular matrix and receptors. Meanwhile, the interaction-induced altered second-messenger-mediated signalling was functionally consistent with the original goal of our experiment, which was to inhibit downstream signalling by blocking Stra6 receptor activity. To confirm whether there are actual interactions between stromal cells and other cells during implantation, we additionally performed single-cell transcriptome sequencing and the results showed that a large number of cellular crosstalk exists between stromal cells and other cells in mice decidua tissues (Figure 8A–H). Interestingly, we found that the number of cellular crosstalk in anti-Stra6-treated decidua was about double that of the control group (Figure 8H), which may be caused by the re-remodeling of decidua tissue. Analyzing differentially expressed genes in decidual stromal cells after anti-Stra6 treatment, we found that these genes were enriched in some metabolic processes, extracellular matrix and structural organization (Figure 8I and J), and were enriched in that genes dynamically change in SC1 cells during pig embryo implantation (Figure S9J and K in Supporting Information). These results revealed that stromal cells are critical in endometrial remodeling (Bourdiec et al., 2013). Collectively, during embryo implantation, Stra6 receptors on endometrial stromal cells may induce the interaction between themselves and other endometrial cells by receiving Rbp4 signals from the embryo to promote endometrial remodeling, resulting in accepted embryo implantation.

In addition, we downloaded data on human blastocysts (Yang et al., 2021) and associated endometrium (Wang et al., 2020) from public databases for analysis. Notably, the expression level of RBP4 in human blastocysts was not high, although it had a tendency to gradually increase with pregnancy development

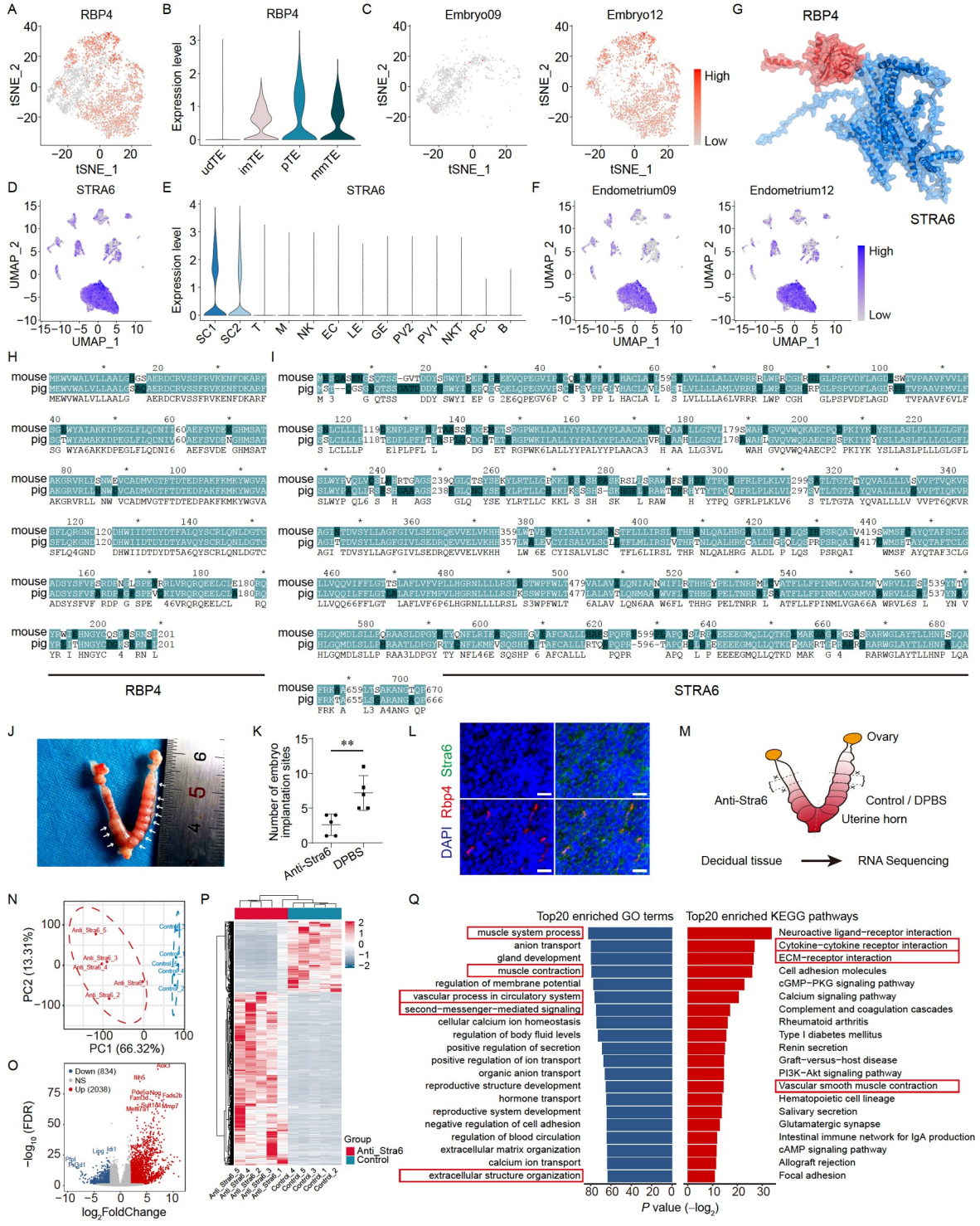

Figure 7. Embryonic trophoblast-derived RBP4 targets endometrial type 1 stromal cell surface receptor STRA6 to promote the interaction between endometrial stromal cells and other cells. A, The distribution of RBP4 expression in TE cells on tSNE. B, Violin plots showing the RBP4 expression levels in each TE subpopulation. C, tSNE representation of RBP4 expression in embryonic TEs on days 9 and 12 of pregnancy. D, The distribution of STRA6 expression in endometrial cells on UMAP. E, Violin plots showing the STRA6 expression levels in each type of endometrial cells. F, UMAP representation of STRA6 expression in endometrial cells on days 9 and 12 of pregnancy. G, Predicted RBP4 and STRA6 binding site models using AlphaFold2. The red part represents RBP4, and the blue part represents STRA6. H, Amino acid sequence alignment of mouse and pig RBP4 proteins. I, Amino acid sequence alignment of mouse and pig STRA6 proteins. J, Representative images of E6.5 embryo implantation sites after injection of anti-Stra6 (left) or DPBS (right) into mouse uterine horns. White arrows indicate implanted mouse embryos. K, Comparison of the number of E6.5 embryo implantation sites after injecting anti-Stra6 or DPBS into mouse uterine horns. Data are presented using mean±SEM (n=5), paired two-sided t test. **, P<0.01. L, Representative immunofluorescence costaining images of Rbp4 and Stra6 in E6.5 mouse uterus. Scale bar, 20 μm. M–Q, Bulk transcriptome analysis of decidua tissue after injection of anti-Stra6 in mice uterus. M, Schematic showing the isolation of decidual tissue from E6.5 mouse uterus. The myometrium and embryo were removed. N, Principal component analysis of mouse decidual tissue. O, Volcano plot of differentially expressed genes. P, Heatmap of differentially expressed genes. Q, GO enrichment and KEGG pathway analysis of differentially expressed genes, showing the top 20 enriched terms for each category.

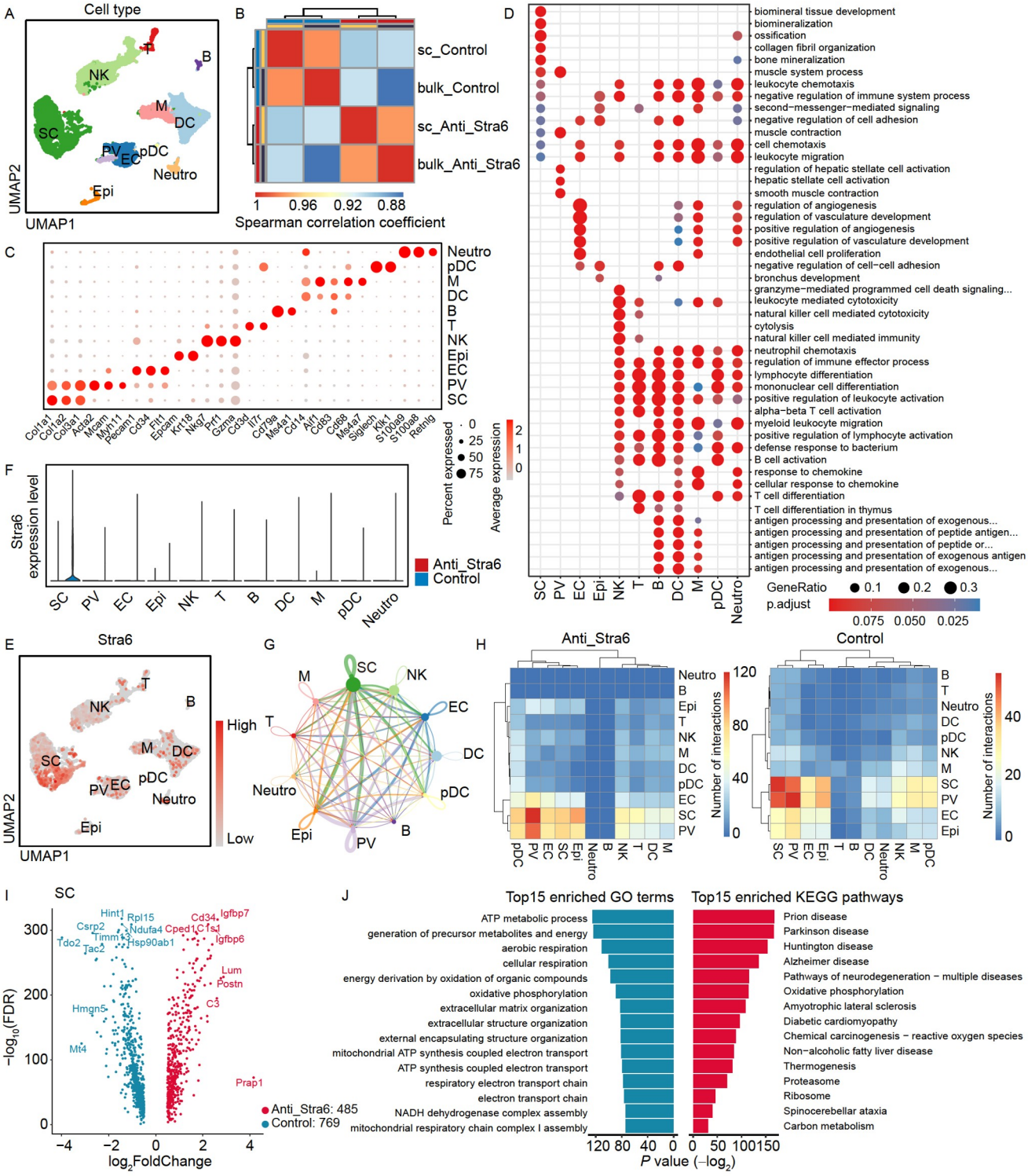

Figure 8. Single-cell transcriptome analysis of decidua tissue after mice uterine injection with anti-Stra6. A, UMAP of cells coloured by associated cell types in mice decidua tissue. B, B cells; DC, dendritic cells; EC, endothelial cells; Epi, epithelial cells; M, macrophages; Neutro, neutrophils; NK, natural killer cells; pDC, plasmacytoid dendritic cells; PV, perivascular cells; SC, stromal cells; T, T cells. B, Correlation analysis of merged decidua cells compared with bulk transcriptomes. C, Dot plots showing the expressed and coexpressed classical marker genes of each cell type. D, Top 5 enriched GO biological process terms of the most significant 50 decidua cells-specific genes. E, The distribution of STRA6 expression in decidua cells on UMAP. F, Violin plots showing the STRA6 expression levels in each type of decidua cells. G, Circle plots showing the number of inferred interactions between different type of decidua cells using CellChat. H, Heatmap showing the number of inferred interactions between different types of decidua cells using CellChat in anti-Stra6 treated and control uterus. I, Volcano plot showing differentially expressed genes in anti-Stra6 treated and control decidual tissue SC cells. J, GO enrichment and KEGG pathway analysis of differentially expressed genes in anti-Stra6 treated and control decidual tissue SC cells, showing the top 15 enriched terms for each category.

https://doi.org/10.1007/s11427-023-2557-x

(Figure S12H–K in Supporting Information). This is likely because the human embryos used for the study were not developed *in vivo* but cultured *in vitro*. Similar to that in pigs or mice, the STRA6 receptor is specifically expressed in human endometrial stromal cells, with increased expression levels from the proliferative to secretory phase (Figure S12L–O in Supporting Information), implying that the RBP4/STRA6 pathway in intrauterine maternal-foetal crosstalk may be conserved in mammals.

Disorders of maternal-foetal crosstalk have profound implications for women's health and reproductive outcomes. In the past decade, research progress on these disorders has been limited, partly because of the challenges of analysing the precise and complex maternal-foetal crosstalk. In the present study, the expression level of the conserved endometrial stromal cell receptor STRA6 we identified was significantly lower in recurrent pregnancy failure (Lai et al., 2022) and thin endometrial stromal cells (Lv et al., 2022) than in normal endometrium (Figure S13A–I in Supporting Information), suggesting that a disorder of maternal-foetal crosstalk mediated by the RBP4/STRA6 pathway could indeed lead to adverse pregnancy-related outcomes.

Together, our data suggest that the RBP4/STRA6 pathway regulates the interaction of endometrial stromal cells with other cells during pregnancy across species and that low-level expression of the STRA6 receptor, which is specifically expressed in endometrial stromal cells, contributes to the disruption of maternal-foetal crosstalk. This could lead to pregnancy abnormalities, including recurrent pregnancy failure and a thin endometrium.

DISCUSSION

In this study, we comprehensively characterized the cellular profiles of pig embryos and the corresponding endometrium at two peri-implantation stages. By integrating the uterine luminal fluid protein abundance profiles from our previous studies, we revealed global crosstalk between embryos and the mother during implantation through the developed tool ExtraCellTalk using transcriptional differences in two-stage embryos and endometrial cells, which helped improve our understanding of embryo implantation. Through these analyses, we found that the RBP4/STRA6 pathway may be essential during implantation. Our study provides unique insights into maternal-foetal crosstalk during implantation, which is critical for our fuller understanding of how maternal-foetal processes are coordinated during pregnancy, and future studies may facilitate the development of effective strategies to reduce pregnancy loss.

Due to experimental difficulties and technical limitations, most previous studies on embryo implantation focused solely on embryos or endometrium and only at the overall tissue level (Hamatani et al., 2004; Smith et al., 2011). In fact, successful pregnancy is a dynamic process that requires precise synchronization and coordination between the embryo and the mother to complete timely implantation of semi-allogeneic embryos (Ye et al., 2005). To understand the molecular regulation of embryo implantation more truthfully, a simultaneous study of the embryo and the maternal uterus is needed. Moreover, due to the complexity of endometrial tissue, it is also necessary to dissociate the tissue to analyse heterogeneous cells (Suhorutshenko et al., 2018). With advances in single-cell sequencing technology, recent studies have revealed the interaction between the extravillous trophoblast and decidua by sampling placental tissue from the maternal-foetal interface (Vento-Tormo et al., 2018) and human endometrial transformation by collecting endometrial tissue across the menstrual cycle (Wang et al., 2020). Unfortunately, these studies have not clearly elucidated maternal-foetal crosstalk overall. Indeed, considering ethical and other constraints, it is impractical to study this issue in humans, and due to species differences, using a single animal model may lose some vital information. Therefore, we chose another excellent animal model pigs besides mice, collected contemporaneous embryos and endometrial tissue to comprehensively characterize the dynamic crosstalk between embryos and the maternal endometrium during implantation, and conducted cross-species comparisons to provide a unique perspective.

Since Vento-Tormo et al. (2018) developed CellPhoneDB to predict the communication between different cells from single-cell transcriptome data, a growing number of tools have been developed using different algorithms for the prediction of cell communication, such as CellChat (Jin et al., 2021) and NicheNet (Browaeys et al., 2020). Unfortunately, these tools are all designed to predict ligand-receptor signalling pathways between different cells in adjacent tissues. For semi-allogeneic embryos, it does not appear to be reliable to predict long-distance communication with the maternal endometrium by direct use of these tools. Therefore, in this study, we considered introducing an external variable as a predictive bridge for long-distance cellular communication. Substances in the microenvironment of the uterine lumen are believed to mediate maternal-foetal crosstalk (Salamonsen et al., 2016). In view of the potential functional mechanisms of different substances, we finally selected proteins directly involved in biological functions as the bridge between the embryo and the maternal uterus. On this basis, we developed a novel tool, ExtraCellTalk, which predicts long-distance cell communication by introducing uterine lumen proteins as external variables through ligand-receptor complexes. However, there are two different forms of proteins within the uterine lumen, either free or encapsulated in extracellular vesicles. Cell surface proteins and intracellular proteins are involved in many different biological processes; thus, the tool provides appropriate methods to make proper predictions. Through ExtraCellTalk, we gained a comprehensive understanding of the crosstalk between embryos and the mother during implantation in pigs, which is of great reference value for an in-depth understanding of embryo implantation. Furthermore, this form of free protein or extracellular vesicles is ubiquitous in various biological processes (Proctor, 2016; Robbins and Morelli, 2014), so the tool is further suitable for predicting other diverse long-distance cellular communications. Collectively, our findings provide a new perspective for cell communication prediction that is not limited only to proteins but has the possibility to lead to a better understanding of cell communication mediated by other RNA molecules in the future.

Among all uterine luminal protein-mediated maternal-foetal crosstalk pathways, the RBP4/STRA6 pathway was singled out for scrutiny because of its highest ExtraCellTalk score and features conserved across species. Previous studies on the RBP4/STRA6 pathway have focused mainly on the transportation of retinol by the retinol-RBP4 complex and STRA6 receptor recognition, and the subsequent activated STRA6-mediated cell signal transduction (Gliniak et al., 2017; Huang et al., 2021;

Noy, 2016). In diseases such as obesity, these signalling cascades may regulate insulin resistance, and researchers suggest that this pathway may represent a novel therapeutic target for the treatment of metabolic diseases. Our study proved that the pathway is also critical during embryo implantation and that blocking the activity of the STRA6 receptor can lead to endometrial re-remodelling and embryo loss. This may be partly caused by the failure of the transformation of endometrial stromal cells due to aberrant retinoic acid metabolism (Nakajima et al., 2016). Meanwhile, it may also be because of the blockade of STRA6 receptor-mediated cell signalling, resulting in the absence of downstream signals and abnormal crosstalk between stromal cells and other cells (Sidell et al., 2010). This ultimately leads to failure of endometrial remodelling and pregnancy, suggesting that STRA6 is a potential functional target for contraceptives. Other identified pathways, such as trophoblast-derived IFNG could target CDH1 on the surface of endometrial LE cells to function (Figure 6D). Previous studies have found that pig trophoblast-derived IFNG can modify tight junctions in the maternal epithelium (Cencič et al., 2003). As a single-span transmembrane glycoprotein, CDH1 is a member of the cadherin superfamily of cell adhesion molecules that regulates the structural development of epithelial differentiation and intercellular adherens junctions (Reardon et al., 2012). This implies that pig trophoblast-derived IFNG is likely to change maternal epithelial cell tight junctions through the IFNG/CDH1 pathway. In summary, we demonstrated that the pig model provides a robust basis for exploring the crosstalk between embryos and the mother during implantation.

Mismatched developmental timing between the fertilized embryo and uterus prevents successful embryo implantation, leading to pregnancy failure, whereas crosstalk between the embryo and mother coordinates their synchronized development (Chen et al., 2011). In this study, our pig model showed that embryos undergo dynamic crosstalk with the mother's uterus during implantation. With the development of reproductive medicine, although the success rate of *in vitro* fertilization and embryo transfer has significantly improved compared with the previous rates, the failure rate is still high (Carson and Kallen, 2021). The reason for this is most likely caused by the lack of adequate crosstalk between embryo and the maternal endometrium. This needs to be further confirmed by follow-up studies to make a great contribution to overcoming infertility. Additionally, pregnancy failure in domestic animals, including pigs, sheep, and cattle, also majority occurs during implantation (Rickard et al., 2017; Wiltbank et al., 2016). Our identification of molecular regulatory mechanisms that synchronize coordination between the developing embryos and endometrium highlights the establishment of communication between the trophoblast and the endometrium during embryo implantation, which greatly promotes the understanding of embryo implantation in livestock animals and provides a valuable resource for further reducing embryo loss rates.

In conclusion, this analysis systematically depicts the crosstalk between embryos and the mother during implantation, providing new insights into the regulation of embryo implantation, and may help accelerate research to overcome reproductive difficulties and further improve the success rate of assisted reproduction in the future. Furthermore, we developed ExtraCellTalk and provided a method for building intermediate molecular bridges to reveal long-distance cellular communication, which will contribute to a better understanding of biological development, disease pathogenesis, and other important processes.

MATERIALS AND METHODS

Experimental models and biological samples

All animal experiments and procedures in this study were approved by the Ethics Committee of the Laboratory Animal Center of South China Agricultural University (permit number: SYXK-2022-0136). The animals requiring slaughter were humanely euthanized as necessary to relieve suffering.

Healthy and disease-free Yorkshire sows (parity 2) from commercial farms were checked for oestrus twice daily and artificially inseminated after oestrus with a standard dose of single Yorkshire semen. The day of artificial insemination was marked as day 0 of pregnancy. Six Yorkshire sows were randomly divided into two groups. Sows were slaughtered on days 9 (n=3) and 12 (n=3) of pregnancy, and the uterus was immediately transported to the laboratory in an icebox. Pig embryos on days 9 and 12 of pregnancy were collected from bilateral uterine horns, while corresponding endometrial and uterine section samples were collected from each uterine horn on the anti-mesometrial side of the uterus. Uterine section samples were subsequently fixed in 4% paraformaldehyde for 24 h, embedded in paraffin, and sectioned for immunohistochemistry and immunofluorescence. For embryos, a total of approximately 30 embryos from three sows per stage were pooled for tissue dissociation and single-cell suspension preparation. For the endometrium, the endometrial tissues collected from different positions of the uterine horns of three sows were also mixed for the preparation of single-cell suspension.

Specific pathogen-free (SPF) ICR mice were purchased from Guangdong Medical Laboratory Animal Center (Guangzhou, China). The mice were then used for timed mating, with the morning of vaginal plug appearance recorded as E0.5. On E3.5, each uterine horn of the female mice was slowly injected with 5 μL of 90 μg mL^{-1} anti-Stra6 (Proteintech, Wuhan, China) or DPBS using a microsyringe (Hamilton, Germany). On E6.5, the treated mice were sacrificed to count the number of implanted embryos, and decidua samples from the embryos removed were collected separately from the uterine horns on both sides of the mice. Some were used to dissociate the tissue and obtain the single-cell suspension, and the remainder were snap-frozen in liquid nitrogen and stored at −80°C.

Tissue dissociation and single-cell suspension preparation

Samples were rinsed several times with DPBS, minced into small pieces with scissors, and transferred to precooled EP tubes. For embryos, the minced tissues were digested in prewarmed enzyme cocktail I, which contains papain, dispase and DNase I, at 37°C for 30 min. Endometrial and decidua tissues were digested in enzyme cocktail II, including type II collagenase, type IV collagenase, dispase and DNase I. The dissociatation reaction was terminated with DMEM containing 10% foetal bovine serum (FBS),and then, the cell suspension was passed through a 70-μm sterile cell strainer and centrifuged at 500×g for 5 min at 4°C. After the supernatant was removed, the pelleted cells were suspended in red blood cell lysis buffer and incubated at room temperature for 5 min to exclude remaining red blood cells.

Finally, the cell pellets were washed twice and resuspended in DPBS containing 0.04% bovine serum albumin (BSA) for further single-cell RNA sequencing analysis.

Single-cell RNA-seq library generation and sequencing

The concentration of single-cell suspensions was adjusted to approximately 1,000 cells/μL using DPBS containing 0.04% BSA. Then, single-cell suspensions were loaded on a Chromium Single Cell Controller (10X Genomics, USA) according to the manufacturer's instructions (Chromium Next GEM Single Cell 3′ Reagent Kit V3 User Guide). All subsequent steps were performed following the standard manufacturer's protocols. Purified libraries were analysed by the Illumina NovaSeq 6000 platform using a paired-end 150-bp sequencing strategy and aiming for 25,000 paired reads per cell.

Pre-processing single-cell RNA-seq data

The 10X Genomics scRNA-seq data were processed to quantify gene counts using the Cell Ranger pipeline (v.6.1.2) with default parameters. First, binary base call (BCL) files generated by the NovaSeq 6000 sequencing system were converted to standard FASTQ files using the mkfastq function in Cell Ranger. The pig reference genome and gene annotation files (Sscrofa11.1) were downloaded from the Ensembl website (http://asia.ensembl.org/index.html) and indexed using the mkref function. Mouse reference genome and gene annotation files were obtained directly from the 10X Genomics website. Subsequently, cell number and gene counts in the library were determined using the count function. Further downstream analyses were performed in the R package Seurat (v.4.0.5) (Butler et al., 2018).

Quality control of single-cell RNA-seq data

Stringent quality filter criteria were achieved to filter out low-quality cells based on four metrics: the number of detected genes, unique molecular identifier (UMI) counts, percentage of mitochondrial gene expression, and genes per UMI across cells. Specifically, cells expressing at least 200 genes and having a mitochondrial gene count of less than 20% were used for follow-up analysis. Only genes expressed by more than three cells were kept for subsequent analyses.

Dimension reduction and unsupervised clustering

Highly variable genes (HVGs) were calculated by the SelectIntegrationFeatures function in Seurat, using the parameter nfeature=5,000. Subsequently, the SCTransform function (Hafemeister and Satija, 2019) was used to integrate datasets of different stage samples with default parameters. Following PCA, a UMAP was generated by the RunUMAP function using 40 dimensions, which reveals the principal axes of variation. Different tissue samples were clustered unsupervisedly using the FindClusters function with an appropriate resolution that captured most of the biological variance without oversplitting the data. The type of individual cells was determined based on well-known classical cell-specific markers. Differences between identified cell types at different stages were assessed using the Pearson correlation coefficient.

Signature score calculation

To assess the status of four lineages identified in pig embryos, we calculated lineage scores per single cell using lineage-specific genes in pig embryos previously identified in published data (Zhi et al., 2022). Average overexpression of lineage signatures was calculated using the AddModuleScore function and then normalized between 0-100 to assess the lineage score for each cell. The "ggtern" package (v.3.3.5) was used to visualize and transform the three-dimensional axis into two dimensions. Furthermore, polar, mural and stemness signature scores for all TE cells were also calculated using the AddModuleScore function.

Transcription factor regulon analysis

The analysis of transcription factor regulons in TE cell subsets was performed using pySCENIC (v.0.12.0) (Van de Sande et al., 2020). Loom file output by pySCENIC was analysed by the ScopeLoomR R package (v.0.13.0), and active regulons were then identified based on the output area under the recovery curve (AUC) values and AUC thresholds.

Endometrial stromal and immune cell score calculation

To verify the accuracy of the 13 endometrial cell clusters identified, we used an ESTIMATE algorithm (v.1.0.13) (Yoshihara et al., 2013) to separately assess the stromal and immune scores for different cell clusters. As expected, the corresponding types of cells exhibited stromal or immune states. This further validates the rationality of the endometrial cell clusters we identified.

Differentially expressed gene identification

Genes that were specifically expressed between diverse cell types were identified with the FindAllMarkers function, using a MAST test with the parameters "logfc.threshold=0.5, min.pct=0.25, only.pos=TRUE". The top genes were used as signature genes and visualized using ComplexHeatmap (v.2.10.0).

GO enrichment and KEGG pathway analysis

The GO enrichment and KEGG pathway analysis of genes were implemented by the R package clusterProfiler (v.4.2.1) (Wu et al., 2021), and the top enriched GO terms and KEGG pathways were visualized by ggplot2.

Differentiation trajectory inference

RNA velocity analysis

Loom files of spliced and unspliced expression matrices were generated using the Python program velocyto (v.0.17.17) with default parameters (La Manno et al., 2018). The pig low-complexity and repetitive regions were downloaded from the UCSC Browser (http://genome.ucsc.edu/, on 14 March 2022). The object was then filtered to exclude cells previously removed during quality control. Following filtration, RNA velocity was computed by scVelo (v.0.2.4) with the parameters "min_shared_counts=20, n_top_genes=2000, n_pcs=30, n_neighbors=30, mode=deterministic" (Bergen et al., 2020). The embedding used was UMAP obtained in the previous section.

Pseudotime construction

The Monocle2 algorithm (v.2.22.0) (Qiu et al., 2017) was used to construct the pseudotime trajectory on selected cell populations. The eigengenes calculated by the differentialGeneTest function (q value<0.01) were selected as ordering genes to sort cells into pseudotime order. A discriminative dimensionality reduction with trees (DDRtree) method was used to reduce dimensionality using the reduceDimension function with the parameter "max_components=2". Cell developmental trajectories were subsequently inferred using default parameters.

CytoTRACE analysis

We used the R package CytoTRACE (v.0.3.3) (Gulati et al., 2020) to identify differences in transcriptional diversity during cell differentiation, thereby calculating CytoTRACE scores for each cell to predict the differentiation state. CytoTRACE scores range from 0 to 1, with higher scores generally indicating higher stemness (less differentiation), the results of which could complement the trajectory inference of Monocle2.

CellChat analysis

To gain a comprehensive understanding of cell-cell communication, CellChat (v.1.15.0) (Jin et al., 2021) was used to infer the crosstalk between each cell type in tissues.

Comparative integrative analysis of single-cell RNA-seq data

Because EPI in the early embryos of different species is relatively conserved, we intend to analyse the consistency of early embryo stages across species using EPI data. First, for pigs, the EPI data of early pig embryos from Zhi et al. (2022) and Liu et al. (2021a) were extracted and integrated with our EPI data. We used co-expressed genes from all three datasets as anchors, followed by using the removeBatchEffect function in limma (v.3.50.1) (Smyth, 2005) to remove batch effects between different datasets. The Pearson correlation coefficient was finally used to measure the consistency between our data and those previously published by others. For mice and humans, the EPI data of early mouse embryos from Mohammed et al. (2017) and early human embryos from Zhou et al. (2019) were also extracted and integrated in the same way, and the Pearson correlation coefficients were calculated to assess the consistency of early embryo stages across species. Note that the common gene symbol was used to determine the co-expressed genes in different datasets.

In the analysis of the RBP4/STRA6 pathway during maternal-foetal crosstalk, the determination of RBP4 expression levels in mouse and human embryos was also derived from the above-mentioned studies by Mohammed et al. and Zhou et al. The expression of STRA6 in mouse and human endometrium was derived from the single-cell transcriptome data of mouse early pregnancy endometrium by Yang et al. (2021) and human menstrual cycle endometrium by Wang et al. (2020), respectively. Using the study by Lai et al. (2022) on recurrent pregnancy failure, we analysed STRA6 expression levels in the endometrium of normal pregnancy versus recurrent pregnancy failure. The significance of the differential expression of STRA6 in the endometrial stromal cells of normal pregnancy versus recurrent pregnancy failure was assessed by unpaired two-sided Wilcoxon test. Similarly, we analysed STRA6 expression levels in normal versus thin endometrium using single-cell RNA-seq from Lv et al. (2022).

Bulk RNA sequencing and analysis

Total RNA of mouse decidua tissues was extracted using TRIzol reagent (Invitrogen, USA), and sequencing libraries were prepared using the NEBNext Ultra RNA Library Prep Kit for Illumina (New England BioLabs, USA) according to the manufacturer's instructions, followed by sequencing on a NovaSeq 6000 platform to generate 150-bp paired-end sequencing reads.

The raw reads obtained by sequencing were trimmed to obtain high-quality clean reads by removing adapter sequences, reads with unknown bases, and low-quality reads. These clean reads were aligned to the mouse reference genome (GRCm39) using HISAT2 (v.2.0.5) (Mortazavi et al., 2008), and the matched reads were used to assemble transcripts using StringTie (v.1.3.3b) (Pertea et al., 2015). Finally, the count of each gene was quantified using featureCounts (v1.5.0-p3) (Liao et al., 2014). Based on the gene length, we normalized the quantitatively obtained gene count to the TPM value for subsequent analysis. Differential expression analysis of genes between the experimental and control groups was performed using the DESeq2 R package (v.1.34.0) (Love et al., 2014), and significant differential genes were determined by FDR values (P value adjusted by the Benjamini-Hochberg method (Benjamini and Hochberg, 1995)) <0.05 and $|\log_2(\text{FoldChange})|>2$. GO enrichment and KEGG pathway analysis of differentially expressed genes were also implemented by clusterProfiler.

Single-cell and bulk RNA-seq data integration analysis

To integrate the pig peri-implantation embryos and endometrium sample single-cell datasets in this study with our previously published embryo bulk data (Zang et al., 2021) and the endometrial bulk datasets published by Wang et al. (2016), we performed the following procedures. Raw counts of all cell types in each sample were aggregated as a pseudobulk sample, and the counts per million (CPM) values were then calculated to normalize the library size. For bulk RNA-seq datasets, transcripts per million (TPM) values were used to normalize the gene length and sequencing library size. Subsequently, the removeBatchEffect function in limma (v.3.50.1) (Smyth, 2005) was used to remove batch effects between libraries. We used Spearman correlation coefficients to measure the correlation between single-cell and bulk RNA-seq datasets, and the correlation coefficients were visualized using pheatmap (v.1.0.12). The same procedure was used for the integration of mouse decidua tissue.

Comparative analysis of uterine luminal proteins

Uterine luminal free protein and extracellular vesicle encapsulated protein abundance data on days 9 and 12 of pregnancy were derived from our previously published studies (He et al., 2022; Hong et al., 2023). Proteins were classified according to whether they belonged to uterine luminal free protein or extracellular vesicle encapsulated protein categories. Subcellular localization analysis of classified proteins was performed using DeepLoc (v.2.0, https://services.healthtech.dtu.dk/service.php?

DeepLoc-2.0) (Thumuluri et al., 2022). GO enrichment and KEGG pathway analyses of the proteins were also performed using clusterProfiler as described above. The biological structure of the RBP4/STRA6 complex was predicted by AlphaFold2 (https://github.com/lucidrains/alphafold2).

ExtraCellTalk

To systematically analyse the crosstalk between embryo and the maternal uterus during implantation, we developed ExtraCellTalk, a tool for predicting long-distance cell communication mediated by extracellular proteins as intermediate bridges. The tool is based on the prediction of protein ligands, receptors and their interactions, similar to other previously released prediction tools for cell communication, but extracellular proteins are introduced as intermediate bridges for prediction.

First, we integrated previously released ligands, receptors, and interaction pairs from public databases to obtain more comprehensive annotation information to form ExtraCellTalk's prior knowledge repository, including OmniPath (Türei et al., 2021), CellTalkDB (Shao et al., 2021), NATMI (Hou et al., 2020), CellChat (Jin et al., 2021), SingleCellSignalR (Cabello-Aguilar et al., 2020), ICELLNET (Noël et al., 2021), NicheNet (Browaeys et al., 2020), iTalk (Wang et al., 2019), CellPnoneDB (Efremova et al., 2020), CellCellInteractions (Ximerakis et al., 2019), IUPHAR (Pawson et al., 2014), and several other ligand-receptor pairs included in published articles (Choi et al., 2015; Pavličev et al., 2017; Qiao et al., 2014; Ramilowski et al., 2015). We removed the redundant ligand-receptor interaction pairs, and some complex ligand and receptor complexes were included.

Extracellular proteins were considered interacting ligands. Considering the existing forms of extracellular proteins, the free proteins in this tool were intended to interact with the membrane receptors expressed by the recipient cells, while the proteins encapsulated in extracellular vesicles directly entered the recipient cells and targeted cytoplasmic receptors to influence downstream functions. The membrane and cytoplasmic protein receptors were annotated as previously described (Vento-Tormo et al., 2018). Plasma membrane proteins were downloaded from UniProt using KW-1003 (cell membrane). Peripheral proteins from the plasma membrane were annotated using the UniProt keyword SL-9903, and the remaining proteins were considered transmembrane proteins of extracellular signalling receptors. Cytoplasmic proteins that act as intracellular signalling receptors were downloaded from UniProt using KW-0964 (cytoplasm).

Based on the abundance data of extracellular ligand proteins and the single-cell transcriptome data of recipient cells, ExtraCellTalk calculated the communication scores (S_{lr}) of enriched ligand-receptor pairs in each recipient cell type. Given a recipient cell type i and a pair of ligand-receptor interactions in which the ligand was denoted as l and the receptor was denoted as r, we denoted FC_l as the abundance fold change of ligand protein l and FC_r^i as the expression fold change of receptor gene r in cell type i of the experimental group. Then, the communication score S_{lr} was calculated as follows:

$$S_{lr} = FC_l * FC_r^i.$$

The communication score was calculated for all recipient cell types and for each ligand-receptor interaction pair. To identify specific interactions between ligand and recipient cells, we only considered receptors expressed in more than 25% of the cells in the particular recipient cluster. Users are allowed to change the ratio of receptors expressed in cell clusters. To assess statistical significance, we randomly shuffled the cluster labels of all recipient cells by default 1,000 times and applied the same method to calculate the shuffled communication score. Users are allowed to change the times of cluster label shuffling. Each ligand-receptor pair for each receptor cell type generated a statistical null distribution, followed by a permutation test to obtain a P value for the likelihood of cell-type specificity of a given ligand-receptor complex, and the FDR values were obtained by correcting P values using the Benjamini-Hochberg method (Benjamini and Hochberg, 1995). For ligands and receptors of multisubunit complexes, we required that at least half of the subunits of the complex are expressed. Finally, given the potential cellular origin of the ligand proteins, we calculated the communication score in the same way and obtained a complete network of long-distance cellular communication mediated by extracellular proteins.

Immunohistochemistry

Four micrometre-thick sections from 4% paraformaldehyde-fixed and paraffin-embedded endometrial tissues were dewaxed and hydrated, and endogenous peroxides were quenched with 3% H_2O_2. Subsequently, sections were blocked with 5% BSA (Sigma-Aldrich, USA) and incubated with primary antibodies overnight at 4°C. The primary antibody was replaced with an equal concentration of mouse or rabbit IgG as a negative control. After incubation with the secondary antibody, sections were counterstained with haematoxylin (Thermo Fisher Scientific, Shanghai, China). A Nikon microscope 80i with a DS-Fi1 digital camera (Nikon, Japan) was used for visualization. The antibodies used in this study are listed in Table S5 in Supporting Information.

Immunofluorescence

Embryos were fixed with 4% paraformaldehyde for 30 min at room temperature, permeabilized with 0.5% Triton X-100 (Sigma-Aldrich) in DPBS for 30 min, and blocked by using blocking buffer (3% BSA + 0.1% Tween 20 (Sigma-Aldrich) in DPBS) for 4 h at 4°C. Primary antibodies diluted in blocking buffer were applied to embryos and incubated overnight at 4°C, followed by incubation with diluted fluorescently-conjugated secondary antibodies for 2 h at room temperature in the dark. After labelling, embryos were counterstained with a solution of phalloidin (Thermo Fisher Scientific) and 4′,6-diamidino-2-phenylindole (DAPI, Thermo Fisher Scientific) for 30 min at room temperature. Images were taken using an LSM710 laser confocal scanning microscope (Zeiss, Germany). The antibody information and dilutions used in this study are provided in Table S5 in Supporting Information.

For endometrial tissue staining, sections were dewaxed, hydrated, and quenched for endogenous peroxides as described above for immunohistochemistry. Then, sections were blocked with 3% BSA for 30 min at room temperature and incubated with the primary antibody overnight at 4°C followed by the corresponding secondary antibody for 1 h at room temperature. After the first primary antibody incubation was completed, the primary and secondary antibodies that had been bound to the tissue were removed using Tris-EDTA antigen retrieval buffer

(Servicebio, Wuhan, China), and the second primary antibody was incubated in the same manner. Finally, the nuclei were counterstained with DAPI, and the sections were observed under a microscope.

Data availability

The raw scRNA-seq data of pig embryo and endometrium samples generated in this study are available in the GEO database under accession number GSE222544. The mouse decidua bulk RNA sequencing data used in this study for comparison, are publicly available in the SRA database under accession number PRJNA921903. All other relevant data supporting the key findings of this study are available within the article and its Supplementary Information files. Source data are provided with this paper.

Code availability

ExtraCellTalk is publicly available as a Python program. Source code, as well as tutorials have been deposited in the GitHub repository (https://github.com/xupeng-zang/ExtraCellTalk). Custom scripts for processing and analysing data are available from the corresponding authors upon reasonable request.

Compliance and ethics

The author(s) declare that they have no conflict of interest.

Acknowledgement

This work was supported by the National Key Research and Development Program of China (2021YFD1301103), the National Natural Science Foundation of China (31802033), the Guangdong Provincial Key Area Research and Development Program (2022B0202090002), the Guangdong Basic and Applied Basic Research Foundation (2022A1515011131, 2023A1515030193) and the Guangdong Provincial Promotion Project on Preservation and Utilization of Local Breed of Livestock and Poultry (2018143).

Supporting information

The supporting information is available online at https://doi.org/10.1007/s11427-023-2557-x. The supporting materials are published as submitted, without typesetting or editing. The responsibility for scientific accuracy and content remains entirely with the authors.

References

Albini, A., and Noonan, D.M. (2021). Decidual-like NK cell polarization: from cancer killing to cancer nurturing. Cancer Discov 11, 28–33.

Arck, P.C., and Hecher, K. (2013). Fetomaternal immune cross-talk and its consequences for maternal and offspring's health. Nat Med 19, 548–556.

Bazer, F.W., and Johnson, G.A. (2014). Pig blastocyst-uterine interactions. Differentiation 87, 52–65.

Bazer, F.W., Spencer, T.E., Johnson, G.A., Burghardt, R.C., and Wu, G. (2009a). Comparative aspects of implantation. Reproduction 138, 195–209.

Bazer, F.W., Wu, G., Spencer, T.E., Johnson, G.A., Burghardt, R.C., and Bayless, K. (2009b). Novel pathways for implantation and establishment and maintenance of pregnancy in mammals. Mol Hum Reprod 16, 135–152.

Benjamini, Y., and Hochberg, Y. (1995). Controlling the false discovery rate: a practical and powerful approach to multiple testing. J R Stat Soc 57, 289–300.

Bergen, V., Lange, M., Peidli, S., Wolf, F.A., and Theis, F.J. (2020). Generalizing RNA velocity to transient cell states through dynamical modeling. Nat Biotechnol 38, 1408–1414.

Bourdiec, A., Calvo, E., Rao, C., and Akoum, A. (2013). Transcriptome analysis reveals new insights into the modulation of endometrial stromal cell receptive phenotype by embryo-derived signals interleukin-1 and human chorionic gonadotropin: Possible involvement in early embryo implantation. PLoS ONE 8, e64829.

Brons, I.G.M., Smithers, L.E., Trotter, M.W.B., Rugg-Gunn, P., Sun, B., Chuva de Sousa Lopes, S.M., Howlett, S.K., Clarkson, A., Ahrlund-Richter, L., Pedersen, R.A., et al. (2007). Derivation of pluripotent epiblast stem cells from mammalian embryos. Nature 448, 191–195.

Browaeys, R., Saelens, W., and Saeys, Y. (2020). NicheNet: modeling intercellular communication by linking ligands to target genes. Nat Methods 17, 159–162.

Butler, A., Hoffman, P., Smibert, P., Papalexi, E., and Satija, R. (2018). Integrating single-cell transcriptomic data across different conditions, technologies, and species. Nat Biotechnol 36, 411–420.

Cabello-Aguilar, S., Alame, M., Kon-Sun-Tack, F., Fau, C., Lacroix, M., and Colinge, J. (2020). SingleCellSignalR: inference of intercellular networks from single-cell transcriptomics. Nucleic Acids Res 48, e55.

Carson, S.A., and Kallen, A.N. (2021). Diagnosis and management of infertility: a review. JAMA 326, 65–76.

Cencič, A., Guillomot, M., Koren, S., and La Bonnardière, C. (2003). Trophoblastic interferons: do they modulate uterine cellular markers at the time of conceptus attachment in the pig? Placenta 24, 862–869.

Chen, Q., Zhang, Y., Peng, H., Lei, L., Kuang, H., Zhang, L., Ning, L., Cao, Y., and Duan, E. (2011). Transient β2-adrenoceptor activation confers pregnancy loss by disrupting embryo spacing at implantation. J Biol Chem 286, 4349–4356.

Chen, Y., Clarke, O.B., Kim, J., Stowe, S., Kim, Y.K., Assur, Z., Cavalier, M., Godoy-Ruiz, R., von Alpen, D.C., Manzini, C., et al. (2016). Structure of the STRA6 receptor for retinol uptake. Science 353, aad8266.

Choi, H., Sheng, J., Gao, D., Li, F., Durrans, A., Ryu, S., Lee, S.B., Narula, N., Rafii, S., Elemento, O., et al. (2015). Transcriptome analysis of individual stromal cell populations identifies stroma-tumor crosstalk in mouse lung cancer model. Cell Rep 10, 1187–1201.

Colombo, M., Raposo, G., and Théry, C. (2014). Biogenesis, secretion, and intercellular interactions of exosomes and other extracellular vesicles. Annu Rev Cell Dev Biol 30, 255–289.

Corachán, A., Pellicer, N., Pellicer, A., and Ferrero, H. (2021). Novel therapeutic targets to improve IVF outcomes in endometriosis patients: a review and future prospects. Hum Reprod Update 27, 923–972.

Dey, S.K., Lim, H., Das, S.K., Reese, J., Paria, B.C., Daikoku, T., and Wang, H. (2004). Molecular cues to implantation. Endocrine Rev 25, 341–373.

Du, M.R., Wang, S.C., and Li, D.J. (2014). The integrative roles of chemokines at the maternal-fetal interface in early pregnancy. Cell Mol Immunol 11, 438–448.

Efremova, M., Vento-Tormo, M., Teichmann, S.A., and Vento-Tormo, R. (2020). CellPhoneDB: inferring cell-cell communication from combined expression of multi-subunit ligand-receptor complexes. Nat Protoc 15, 1484–1506.

Geisert, R.D., Whyte, J.J., Meyer, A.E., Mathew, D.J., Juárez, M.R., Lucy, M.C., Prather, R.S., and Spencer, T.E. (2017). Rapid conceptus elongation in the pig: an interleukin 1 beta 2 and estrogen-regulated phenomenon. Mol Reprod Dev 84, 760–774.

Gliniak, C.M., Brown, J.M., and Noy, N. (2017). The retinol-binding protein receptor STRA6 regulates diurnal insulin responses. J Biol Chem 292, 15080–15093.

Gray, C.A., Bartol, F.F., Tarleton, B.J., Wiley, A.A., Johnson, G.A., Bazer, F.W., and Spencer, T.E. (2001). Developmental biology of uterine glands. Biol Reprod 65, 1311–1323.

Gulati, G.S., Sikandar, S.S., Wesche, D.J., Manjunath, A., Bharadwaj, A., Berger, M.J., Ilagan, F., Kuo, A.H., Hsieh, R.W., Cai, S., et al. (2020). Single-cell transcriptional diversity is a hallmark of developmental potential. Science 367, 405–411.

Hafemeister, C., and Satija, R. (2019). Normalization and variance stabilization of single-cell RNA-seq data using regularized negative binomial regression. Genome Biol 20, 1–5.

Hamatani, T., Daikoku, T., Wang, H., Matsumoto, H., Carter, M.G., Ko, M.S.H., and Dey, S.K. (2004). Global gene expression analysis identifies molecular pathways distinguishing blastocyst dormancy and activation. Proc Natl Acad Sci USA 101, 10326–10331.

He, Y.M., Li, X., Perego, M., Nefedova, Y., Kossenkov, A.V., Jensen, E.A., Kagan, V., Liu, Y.F., Fu, S.Y., Ye, Q.J., et al. (2018). Transitory presence of myeloid-derived suppressor cells in neonates is critical for control of inflammation. Nat Med 24, 224–231.

He, Y., Zang, X., Kuang, J., Yang, H., Gu, T., Yang, J., Li, Z., Zheng, E., Xu, Z., Cai, G., et al. (2022). iTRAQ-based quantitative proteomic analysis of porcine uterine fluid during pre-implantation period of pregnancy. J Proteomics 261, 104570.

Hong, L., Zang, X., Hu, Q., He, Y., Xu, Z., Xie, Y., Gu, T., Yang, H., Yang, J., Shi, J., et al. (2023). Uterine luminal-derived extracellular vesicles: potential nanomaterials to improve embryo implantation. J Nanobiotechnol 21, 79.

Hou, R., Denisenko, E., Ong, H.T., Ramilowski, J.A., and Forrest, A.R.R. (2020). Predicting cell-to-cell communication networks using NATMI. Nat Commun 11, 5011.

Huang, R., Bai, X., Li, X., Wang, X., and Zhao, L. (2021). Retinol-binding protein 4 activates STRA6, provoking pancreatic β-cell dysfunction in type 2 diabetes. Diabetes 70, 449–463.

Jin, Q., Yang, X., Gou, S., Liu, X., Zhuang, Z., Liang, Y., Shi, H., Huang, J., Wu, H., Zhao, Y., et al. (2022). Double knock-in pig models with elements of binary Tet-On and phiC31 integrase systems for controllable and switchable gene expression. Sci China Life Sci 65, 2269–2286.

Jin, S., Guerrero-Juarez, C.F., Zhang, L., Chang, I., Ramos, R., Kuan, C.H., Myung, P.,

Plikus, M.V., and Nie, Q. (2021). Inference and analysis of cell-cell communication using CellChat. Nat Commun 12, 1088.
Kaczmarek, M.M., Najmula, J., Guzewska, M.M., and Przygrodzka, E. (2020). MiRNAs in the peri-implantation period: contribution to embryo-maternal communication in pigs. Int J Mol Sci 21, 2229.
La Manno, G., Soldatov, R., Zeisel, A., Braun, E., Hochgerner, H., Petukhov, V., Lidschreiber, K., Kastriti, M.E., Lönnerberg, P., Furlan, A., et al. (2018). RNA velocity of single cells. Nature 560, 494–498.
Lai, Z.Z., Wang, Y., Zhou, W.J., Liang, Z., Shi, J.W., Yang, H.L., Xie, F., Chen, W.D., Zhu, R., Zhang, C., et al. (2022). Single-cell transcriptome profiling of the human endometrium of patients with recurrent implantation failure. Theranostics 12, 6527–6547.
Li, R., Zhong, C., Yu, Y., Liu, H., Sakurai, M., Yu, L., Min, Z., Shi, L., Wei, Y., Takahashi, Y., et al. (2019). Generation of blastocyst-like structures from mouse embryonic and adult cell cultures. Cell 179, 687–702.e18.
Liao, Y., Smyth, G.K., and Shi, W. (2014). featureCounts: an efficient general purpose program for assigning sequence reads to genomic features. Bioinformatics 30, 923–930.
Liu, T., Li, J., Yu, L., Sun, H.X., Li, J., Dong, G., Hu, Y., Li, Y., Shen, Y., Wu, J., et al. (2021a). Cross-species single-cell transcriptomic analysis reveals pre-gastrulation developmental differences among pigs, monkeys, and humans. Cell Discov 7, 8.
Liu, X., Tan, J.P., Schröder, J., Aberkane, A., Ouyang, J.F., Mohenska, M., Lim, S.M., Sun, Y.B.Y., Chen, J., Sun, G., et al. (2021b). Modelling human blastocysts by reprogramming fibroblasts into iBlastoids. Nature 591, 627–632.
Love, M.I., Huber, W., and Anders, S. (2014). Moderated estimation of fold change and dispersion for RNA-seq data with DESeq2. Genome Biol 15, 550.
Lunney, J.K., Van Goor, A., Walker, K.E., Hailstock, T., Franklin, J., and Dai, C. (2021). Importance of the pig as a human biomedical model. Sci Transl Med 13, eabd5758.
Lv, H., Zhao, G., Jiang, P., Wang, H., Wang, Z., Yao, S., Zhou, Z., Wang, L., Liu, D., Deng, W., et al. (2022). Deciphering the endometrial niche of human thin endometrium at single-cell resolution. Proc Natl Acad Sci USA 119, e2115912119.
Lyko, F. (2018). The DNA methyltransferase family: a versatile toolkit for epigenetic regulation. Nat Rev Genet 19, 81–92.
Machtinger, R., Laurent, L.C., and Baccarelli, A.A. (2016). Extracellular vesicles: roles in gamete maturation, fertilization and embryo implantation. Hum Reprod Update 22, 182–193.
Mattson, B.A., Overstrom, E.W., and Albertini, D.F. (1990). Transitions in trophectoderm cellular shape and cytoskeletal organization in the elongating pig blastocyst. Biol Reprod 42, 195–205.
McLendon, B.A., Seo, H., Kramer, A.C., Burghardt, R.C., Bazer, F.W., and Johnson, G. A. (2020). Pig conceptuses secrete interferon gamma to recruit T cells to the endometrium during the peri-implantation period. Biol Reprod 103, 1018–1029.
Mohammed, H., Hernando-Herraez, I., Savino, A., Scialdone, A., Macaulay, I., Mulas, C., Chandra, T., Voet, T., Dean, W., Nichols, J., et al. (2017). Single-cell landscape of transcriptional heterogeneity and cell fate decisions during mouse early gastrulation. Cell Rep 20, 1215–1228.
Mortazavi, A., Williams, B.A., McCue, K., Schaeffer, L., and Wold, B. (2008). Mapping and quantifying mammalian transcriptomes by RNA-Seq. Nat Methods 5, 621–628.
Nakajima, T., Iguchi, T., and Sato, T. (2016). Retinoic acid signaling determines the fate of uterine stroma in the mouse Müllerian duct. Proc Natl Acad Sci USA 113, 14354–14359.
Niakan, K.K., Han, J., Pedersen, R.A., Simon, C., and Pera, R.A.R. (2012). Human pre-implantation embryo development. Development 139, 829–841.
Noël, F., Massenet-Regad, L., Carmi-Levy, I., Cappuccio, A., Grandclaudon, M., Trichot, C., Kieffer, Y., Mechta-Grigoriou, F., and Soumelis, V. (2021). Dissection of intercellular communication using the transcriptome-based framework ICELLNET. Nat Commun 12, 1089.
Noy, N. (2016). Vitamin A in regulation of insulin responsiveness: mini review. Proc Nutr Soc 75, 212–215.
Ochiai, Y., Suzuki, C., Segawa, K., Uchiyama, Y., and Nagata, S. (2022). Inefficient development of syncytiotrophoblasts in the *Atp11a*-deficient mouse placenta. Proc Natl Acad Sci USA 119, e2200582119.
Pavličev, M., Wagner, G.P., Chavan, A.R., Owens, K., Maziarz, J., Dunn-Fletcher, C., Kallapur, S.G., Muglia, L., and Jones, H. (2017). Single-cell transcriptomics of the human placenta: inferring the cell communication network of the maternal-fetal interface. Genome Res 27, 349–361.
Pawson, A.J., Sharman, J.L., Benson, H.E., Faccenda, E., Alexander, S.P.H., Buneman, O.P., Davenport, A.P., McGrath, J.C., Peters, J.A., Southan, C., et al. (2014). The IUPHAR/BPS Guide to PHARMACOLOGY: an expert-driven knowledgebase of drug targets and their ligands. Nucl Acids Res 42, D1098–D1106.
Pertea, M., Pertea, G.M., Antonescu, C.M., Chang, T.C., Mendell, J.T., and Salzberg, S. L. (2015). StringTie enables improved reconstruction of a transcriptome from RNA-seq reads. Nat Biotechnol 33, 290–295.
Petropoulos, S., Edsgärd, D., Reinius, B., Deng, Q., Panula, S.P., Codeluppi, S., Plaza Reyes, A., Linnarsson, S., Sandberg, R., and Lanner, F. (2016). Single-cell RNA-seq reveals lineage and X chromosome dynamics in human preimplantation embryos. Cell 165, 1012–1026.
Proctor, G.B. (2016). The physiology of salivary secretion. Periodontol 2000 70, 11–25.
Qiao, W., Wang, W., Laurenti, E., Turinsky, A.L., Wodak, S.J., Bader, G.D., Dick, J.E., and Zandstra, P.W. (2014). Intercellular network structure and regulatory motifs in the human hematopoietic system. Mol Syst Biol 10, 741.
Qiu, X., Hill, A., Packer, J., Lin, D., Ma, Y.A., and Trapnell, C. (2017). Single-cell mRNA quantification and differential analysis with Census. Nat Methods 14, 309–315.
Ramilowski, J.A., Goldberg, T., Harshbarger, J., Kloppmann, E., Lizio, M., Satagopam, V.P., Itoh, M., Kawaji, H., Carninci, P., Rost, B., et al. (2015). A draft network of ligand-receptor-mediated multicellular signalling in human. Nat Commun 6, 1–2.
Ramos-Ibeas, P., Sang, F., Zhu, Q., Tang, W.W.C., Withey, S., Klisch, D., Wood, L., Loose, M., Surani, M.A., and Alberio, R. (2019). Pluripotency and X chromosome dynamics revealed in pig pre-gastrulating embryos by single cell analysis. Nat Commun 10, 1–7.
Reardon, S.N., King, M.L., MacLean Ii, J.A., Mann, J.L., DeMayo, F.J., Lydon, J.P., and Hayashi, K. (2012). Cdh1 is essential for endometrial differentiation, gland development, and adult function in the mouse uterus. Biol Reprod 86.
Rickard, J.P., Ryan, G., Hall, E., de Graaf, S.P., and Hermes, R. (2017). Using transrectal ultrasound to examine the effect of exogenous progesterone on early embryonic loss in sheep. PLoS ONE 12, e0183659.
Robbins, P.D., and Morelli, A.E. (2014). Regulation of immune responses by extracellular vesicles. Nat Rev Immunol 14, 195–208.
Rohani, M.G., and Parks, W.C. (2015). Matrix remodeling by MMPs during wound repair. Matrix Biol 44-46, 113–121.
Rossant, J., and Tam, P.P.L. (2022). Early human embryonic development: Blastocyst formation to gastrulation. Dev Cell 57, 152–165.
Salamonsen, L.A., Evans, J., Nguyen, H.P.T., and Edgell, T.A. (2016). The microenvironment of human implantation: determinant of reproductive success. Am J Rep Immunol 75, 218–225.
Shao, X., Liao, J., Li, C., Lu, X., Cheng, J., and Fan, X. (2021). CellTalkDB: a manually curated database of ligand-receptor interactions in humans and mice. Brief Bioinf 22, bbaa269.
Shi, M., Chen, Z., Chen, M., Liu, J., Li, J., Xing, Z., Zhang, X., Lv, S., Li, X., Zuo, S., et al. (2021). Continuous activation of polymorphonuclear myeloid-derived suppressor cells during pregnancy is critical for fetal development. Cell Mol Immunol 18, 1692–1707.
Sidell, N., Feng, Y., Hao, L., Wu, J., Yu, J., Kane, M.A., Napoli, J.L., and Taylor, R.N. (2010). Retinoic acid is a cofactor for translational regulation of vascular endothelial growth factor in human endometrial stromal cells. Mol Endocrinol 24, 148–160.
Smith, K., Alnifaidy, R., Wei, Q., and Nieman, L.K. (2011). Endometrial Indian hedgehog expression is decreased in women with endometriosis. Fertility Sterility 95, 2738–2741.e3.
Smith, Z.D., and Meissner, A. (2013). DNA methylation: roles in mammalian development. Nat Rev Genet 14, 204–220.
Smyth, G.K. (2005). Limma: Linear models for microarray data. In: Gentleman, R., Carey, V.J., Huber, W., Irizarry, R.A., and Dudoit, S., eds. Bioinformatics and Computational Biology Solutions Using R and Bioconductor. Statistics for Biology and Health. New York: Springer. 397–420.
Suhorutshenko, M., Kukushkina, V., Velthut-Meikas, A., Altmäe, S., Peters, M., Mägi, R., Krjutškov, K., Koel, M., Codoñer, F.M., Martinez-Blanch, J.F., et al. (2018). Endometrial receptivity revisited: endometrial transcriptome adjusted for tissue cellular heterogeneity. Hum Reprod 33, 2074–2086.
Sun, Y., Yang, Y., Jiang, Z., wang, F., Han, K., Hong, L., Cao, J., and Yu, M. (2022). C/EBP-β contributes to pig endometrial LE receptivity by targeting cell remodeling genes during implantation. Reproduction 164, 269–281.
Suryawanshi, H., Morozov, P., Straus, A., Sahasrabudhe, N., Max, K.E.A., Garzia, A., Kustagi, M., Tuschl, T., and Williams, Z. (2018). A single-cell survey of the human first-trimester placenta and decidua. Sci Adv 4, eaau4788.
Thumuluri, V., Almagro Armenteros, J.J., Johansen, A.R., Nielsen, H., and Winther, O. (2022). DeepLoc 2.0: multi-label subcellular localization prediction using protein language models. Nucleic Acids Res 50, W228–W234.
Turco, M.Y., and Moffett, A. (2019). Development of the human placenta. Development 146, dev163428.
Türei, D., Valdeolivas, A., Gul, L., Palacio-Escat, N., Klein, M., Ivanova, O., Ölbei, M., Gábor, A., Theis, F., Módos, D., et al. (2021). Integrated intra- and intercellular signaling knowledge for multicellular omics analysis. Mol Syst Biol 17, e9923.

Van de Sande, B., Flerin, C., Davie, K., De Waegeneer, M., Hulselmans, G., Aibar, S., Seurinck, R., Saelens, W., Cannoodt, R., Rouchon, Q., et al. (2020). A scalable SCENIC workflow for single-cell gene regulatory network analysis. Nat Protoc 15, 2247–2276.
Veeck, J., Chorovicer, M., Naami, A., Breuer, E., Zafrakas, M., Bektas, N., Dürst, M., Kristiansen, G., Wild, P.J., Hartmann, A., et al. (2008). The extracellular matrix protein ITIH5 is a novel prognostic marker in invasive node-negative breast cancer and its aberrant expression is caused by promoter hypermethylation. Oncogene 27, 865–876.
Vento-Tormo, R., Efremova, M., Botting, R.A., Turco, M.Y., Vento-Tormo, M., Meyer, K.B., Park, J.E., Stephenson, E., Polański, K., Goncalves, A., et al. (2018). Single-cell reconstruction of the early maternal-fetal interface in humans. Nature 563, 347–353.
Wang, W., Vilella, F., Alama, P., Moreno, I., Mignardi, M., Isakova, A., Pan, W., Simon, C., and Quake, S.R. (2020). Single-cell transcriptomic atlas of the human endometrium during the menstrual cycle. Nat Med 26, 1644–1653.
Wang, Y., Wang, R., Zhang, S., Song, S., Jiang, C., Han, G., Wang, M., Ajani, J., Futreal, A., and Wang, L. (2019). Italk: an R package to characterize and illustrate intercellular communication. bioRxiv 507871.
Wang, Y., Xue, S., Liu, X., Liu, H., Hu, T., Qiu, X., Zhang, J., and Lei, M. (2016). Analyses of Long Non-Coding RNA and mRNA profiling using RNA sequencing during the pre-implantation phases in pig endometrium. Sci Rep 6, 20238.
Weis, W.I., and Kobilka, B.K. (2018). The molecular basis of G protein-coupled receptor activation. Annu Rev Biochem 87, 897–919.
Whyte, J.J., Meyer, A.E., Spate, L.D., Benne, J.A., Cecil, R., Samuel, M.S., Murphy, C. N., Prather, R.S., and Geisert, R.D. (2018). Inactivation of porcine interleukin-1β results in failure of rapid conceptus elongation. Proc Natl Acad Sci USA 115, 307–312.
Wilcox, A.J., Weinberg, C.R., O'Connor, J.F., Baird, D.D., Schlatterer, J.P., Canfield, R. E., Armstrong, E.G., and Nisula, B.C. (1988). Incidence of early loss of pregnancy. N Engl J Med 319, 189–194.
Wiltbank, M.C., Baez, G.M., Garcia-Guerra, A., Toledo, M.Z., Monteiro, P.L.J., Melo, L. F., Ochoa, J.C., Santos, J.E.P., and Sartori, R. (2016). Pivotal periods for pregnancy loss during the first trimester of gestation in lactating dairy cows. Theriogenology 86, 239–253.
Wu, B., Wang, Y., Yan, J., Liu, M., Li, X., Tang, F., and Bao, S. (2024). Blastoids generated purely from embryonic stem cells both in mice and humans. Sci China Life Sci 67, 418–420.
Wu, T., Hu, E., Xu, S., Chen, M., Guo, P., Dai, Z., Feng, T., Zhou, L., Tang, W., Zhan, L., et al. (2021). clusterProfiler 4.0: a universal enrichment tool for interpreting omics data. Innovation 2, 100141.
Ximerakis, M., Lipnick, S.L., Innes, B.T., Simmons, S.K., Adiconis, X., Dionne, D., Mayweather, B.A., Nguyen, L., Niziolek, Z., Ozek, C., et al. (2019). Single-cell transcriptomic profiling of the aging mouse brain. Nat Neurosci 22, 1696–1708.
Yang, Y., Zhu, Q., and Liu, J. (2021). Deciphering mouse uterine receptivity for embryo implantation at single-cell resolution. Cell Proliferation 54, e13128.
Ye, X., Hama, K., Contos, J.J.A., Anliker, B., Inoue, A., Skinner, M.K., Suzuki, H., Amano, T., Kennedy, G., Arai, H., et al. (2005). LPA3-mediated lysophosphatidic acid signalling in embryo implantation and spacing. Nature 435, 104–108.
Yoshihara, K., Shahmoradgoli, M., Martínez, E., Vegesna, R., Kim, H., Torres-Garcia, W., Treviño, V., Shen, H., Laird, P.W., Levine, D.A., et al. (2013). Inferring tumour purity and stromal and immune cell admixture from expression data. Nat Commun 4, 1.
Yu, L., Wei, Y., Duan, J., Schmitz, D.A., Sakurai, M., Wang, L., Wang, K., Zhao, S., Hon, G.C., and Wu, J. (2021). Blastocyst-like structures generated from human pluripotent stem cells. Nature 591, 620–626.
Zang, X., Gu, T., Hu, Q., Xu, Z., Xie, Y., Zhou, C., Zheng, E., Huang, S., Xu, Z., Meng, F., et al. (2021). Global transcriptomic analyses reveal genes involved in conceptus development during the implantation stages in pigs. Front Genet 12, 584995.
Zhi, M., Zhang, J., Tang, Q., Yu, D., Gao, S., Gao, D., Liu, P., Guo, J., Hai, T., Gao, J., et al. (2022). Generation and characterization of stable pig pregastrulation epiblast stem cell lines. Cell Res 32, 383–400.
Zhou, F., Wang, R., Yuan, P., Ren, Y., Mao, Y., Li, R., Lian, Y., Li, J., Wen, L., Yan, L., et al. (2019). Reconstituting the transcriptome and DNA methylome landscapes of human implantation. Nature 572, 660–664.
Zhu, H., Li, T., Xu, P., Ding, L., Zhu, X., Wang, B., Tang, X., Li, J., Zhu, P., Wang, H., et al. (2024). Effect of autologous bone marrow stem cells-scaffold transplantation on the ongoing pregnancy rate in intrauterine adhesion women: a randomized, controlled trial. Sci China Life Sci 67, 113–121.
Zhu, Y., Zhou, Z., Huang, T., Zhang, Z., Li, W., Ling, Z., Jiang, T., Yang, J., Yang, S., Xiao, Y., et al. (2022). Mapping and analysis of a spatiotemporal H3K27ac and gene expression spectrum in pigs. Sci China Life Sci 65, 1517–1534.